Circulating Marangoni flows within droplets in smectic films

E. S. Pikina,[1,2,3] M. A. Shishkin,[2,4] K. S. Kolegov,[2,5] B. I. Ostrovskii,[2,6] and S. A. Pikin[6]
[1]*Landau Institute for Theoretical Physics of the RAS, 142432, Chernogolovka, Moscow region, Russia*
[2]*Institute of Solid State Physics of the RAS, 142432 Chernogolovka, Moscow region, Russia*
[3]*Oil and Gas Research Institute of the RAS, 119333 Moscow, Russia*
[4]*HSE University, 101000, Moscow, Russia*
[5]*Astrakhan State University, 414056 Astrakhan, Russia*
[6]*FSRC "Crystallography and Photonics" of the RAS, 119333 Moscow, Russia*

(Received 4 July 2022; accepted 13 October 2022; published 14 November 2022)

We present a theoretical study and numerical simulation of Marangoni convection within ellipsoidal isotropic droplets embedded in free-standing smectic films (FSSFs). The thermocapillary flows are analyzed for both isotropic droplets spontaneously formed in FSSF overheated above the bulk smectic-isotropic transition and oil lenses deposited on the surface of the smectic film. The realistic model for which the upper drop interface is free from the smectic layers, while at the lower drop surface the smectic layering persists is considered in detail. For isotropic droplets and oil lenses this leads effectively to a sticking of fluid motion at the border with a smectic shell. The above mentioned asymmetric configuration is realized experimentally when the temperature of the upper side of the film is higher than at the lower one. The full set of stationary solutions for Stokes stream functions describing the Marangoni convection flows within the ellipsoidal drops are derived analytically. The temperature distribution in the ellipsoidal drop and the surrounding air is determined in the frame of the perturbation theory. As a result, the analytical solutions for the stationary thermocapillary convection are obtained for different droplet ellipticity ratios and the heat conductivity of the liquid crystal and air. In parallel, the numerical hydrodynamic calculations of the thermocapillary motion in drops are made. Both analytical and numerical simulations predict the axially symmetric circulatory convection motion determined by the Marangoni effect at the droplet-free surface. Due to a curvature of the drop interface a temperature gradient along its free surface always exists. Thus, the thermocapillary convection within the ellipsoidal droplets in overheated FSSF is possible for the arbitrarily small Marangoni numbers. Possible experimental observations enabling the checking of our predictions are proposed.

DOI: 10.1103/PhysRevE.106.055105

I. INTRODUCTION

A fluid flow within a drop caused by the temperature-dependent surface tension is called Marangoni convection and was first observed in its classical form by Bénard in a process of formation of the characteristic hexagonal convection patterns in flat fluid films [1]. The onset of thermocapillary convection is determined by a dimensionless Marangoni number, Ma, expressing the ratio of surface tension to viscous forces, which has to reach a certain minimum critical value for instability to occur. The arising convective cells are characterized by a unique critical wave number k_c, which determines the scale of the nonuniformity in the plane of the film. In general, the formation of different cellular flow regimes, including rolls, hexagonal patterns, hydrothermal waves, etc., have been reported for fluid films of different size and geometry [2–6]. An extensive literature on thermocapillary driven flows in fluid films exists and both experimental and theoretical studies are thoroughly reviewed; see, for example, [7–10]. The Marangoni phenomenon is important not only for development of fundamental physics of capillarity and wetting; it is frequently encountered in industrial applications, including chemical engineering, food and cosmetic processing, thermal management of microfluidic and electronic devices, and evaporation-related technology [6,10–12]. Marangoni convection is especially important for thermal processing of electronic and rheological devices in microgravity conditions where buoyancy effects are negligible [13–15].

The past two decades were marked by significant advancements in experimental and theoretical studies of the symmetry and dynamics of Marangoni cellular flows in fluid films of various confinements [6,10,11,16–19]. However, the above mentioned progress largely concerned the Marangoni convection in systems with a variable flat geometry. In spite of its practical and theoretical significance, thermocapillarity at curved fluid interfaces has not caught the proper attention due to its complexity. The convection inside a droplet of a spherical shape [20–27] appears to be principally different from the conventional Marangoni flows in plane films. This is due to the inhomogeneity which is imposed on the interface temperature by the curved shape of the drop. Moreover, the spherical geometry of the drop modifies flow patterns, thus affecting the heat and mass transport within the fluid. The thermocapillary flow within the spherical droplet is usually considered as a

concomitant process in respect of the main physical phenomena occurring in it; a clear example is the evaporation of a sessile liquid drop with a pinning contact line in an ambient air [20–27]. In such a drop the fluid may undergo either outward movement produced by the evaporation-driven flow or a circulatory motion related to the Marangoni effect. One of the few works that carefully analyze the effects of Marangoni flows in evaporating sessile drops with the spherical interface is the classical study by Hu and Larson [21,22]. In their papers, the authors model a convection in a flattened droplet on a partially wetting substrate using both a lubrication analysis and a finite element model (FEM). They found that convective axially symmetric circulatory motions are occurred driven by a nonuniform temperature distribution at the surface of the droplet which arises from evaporative cooling. In the paper by Tam *et al.* [24] a small droplet of water sitting on top of a heated superhydrophobic surface was considered. Similarly to Hu and Larson, the axially symmetric (toroidal) convection patterns were observed in a spherical drop in which the fluid raised along its surface and accelerated downwards in the interior towards the liquid-solid contact point due to the presence of a vertical temperature gradient. The effect of Marangoni forces on the evaporation dynamics of the sessile drops was studied in the theoretical paper by Barash *et al.* [25]. The authors identified various dynamic stages of the thermocapillary convection associated with the generation of the array of convective vortices near the drop surface and their transformation into the single convection vortex over time.

While the fundamentals of Marangoni convection are well established in systems with a simple flat geometry, an analytical description of the thermocapillary flow in fluid drops of ellipsoidal shape is not available yet. In this work we undertake a step in this direction presenting a quantitative description enabling us to account for all relevant aspects of the Marangoni flows in ellipsoidal droplets, namely, the analytical stationary and critical solutions for the Stokes stream functions, the spatial temperature and the velocity distributions for initial stage of the convection. The shape and the axial symmetry of the fluid droplets possessing two spherical interfaces were approximated by an oblate spheroid. Accordingly, elliptical coordinate systems were chosen for the analytical derivations. In addition, the numerical hydrodynamic experiment that models the thermocapillary motion in ellipsoidal drops was conducted. Both the analytical derivations and numerical simulations predict the axially symmetric circulatory convection motion within the droplet determined by the Marangoni effect at the droplet-free surface. The convection patterns represent either individual toroidal-like vortices or series of vortices distributed within the plane of the drop.

Although the developed approach is quite general and thus applies to a wide variety of the Marangoni convection problems in ellipsoidal fluid droplets and bubbles, here we focus on two specific cases. First, we consider isotropic droplets spontaneously generated in free-standing smectic films (FSSFs) heated above the temperature of the bulk smectic-isotropic transition [Fig. 1(a)]. As a second case we consider the droplets of insoluble fluids (of the type of oil or glycerol) which can be deposited on overheated FSSFs in various ways [28–30]. For example, oil vapor can condense at

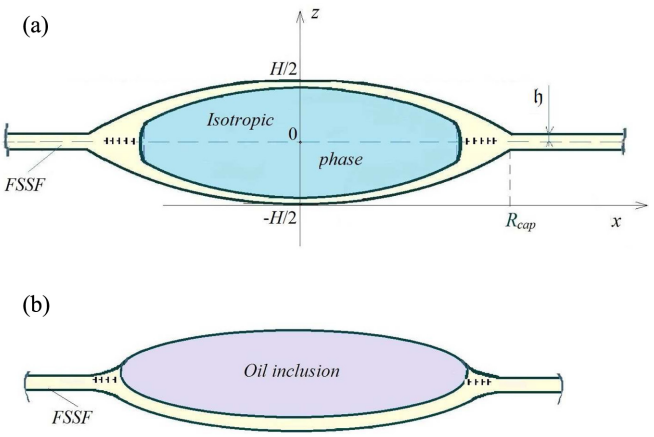

FIG. 1. Schematic view of fluid droplets in free-standing smectic films (FSSFs): (a) isotropic drops formed in overheated FSSFs. The drop is connected with the FSSF of uniform thickness by a meniscus. The drop has a lenslike shape and is symmetric relative to the horizontal plane. The height of the drop and the base radius of the cap are designated as H, $R_{\rm cap}$, respectively. (b) Oil lenses deposited on the surface of FSSFs. In all cases the film thickness ɦ is much smaller than the droplet height.

one of the sides of the smectic film thus forming the lenslike oil drops with the lateral diameter of the order of mm [29,30] [Fig. 1(b)]. The FSSFs are usually made from the smectic A (Sm-A) and smectic C (Sm-C) liquid crystal materials. The Sm-A phase consists of a stack of parallel molecular layers, in which elongated molecules are oriented on average along the layer normal and exhibit the short-range positional order within the layers. The Sm-C phase differs from the Sm-A phase by a tilt of the long molecular axes with respect to the layer normal. Being stretched on a frame, these materials due to their layered structure form free-standing films [31–33] in which the smectic layers align parallel to the two air-film interfaces. The FSSFs can also be prepared as bubbles, either connected with an inflation tube or floating freely under microgravity conditions [34–36]. In many cases the free-standing smectic films can be heated above the bulk smectic disordering temperature without rupturing, and instead show a tendency for the spontaneous nucleation and growth of the isotropic droplets [37–39]. The isotropic droplets have a shape of spherical segments (circular flat lenses), the height of which (of the order up to tens of microns) is about one order of magnitude less than the drop lateral dimension [Fig. 1(a)]. As the FSSF thickness is about a few molecular layers (approximately 100 nanometers), the height of the isotropic droplet is much larger than the film thickness. Thus, such oblate droplets can be viewed as 3D fluid objects embedded into a quasi-2D smectic film which serves as a frame (substrate) for them.

The occurrence of the thermocapillary-driven macroscopic material transport has been previously reported in FSSFs of certain materials [40–43]. The linear temperature gradient in these experiments was applied in the plane of the film, i.e., in the plane of the smectic layers which have a fluid nature. The application of the temperature gradient in the direction along the layer normal in FSSFs, possessing the solidlike

elastic response, has not been taken into consideration for realization of Marangoni transport due to a weak permeation in smectic, where molecules are unable to flow through the smectic layers [44–46]. In our preceding paper [47] we have analyzed the possibility of thermocapillary convection within isotropic droplets spontaneously formed in FSSFs. The horizontal smectic film with isotropic droplets formed in it was expected to be heated either from the bottom, or from the top, thus creating the vertical temperature gradient along the FSSF normal. To calculate the Marangoni number for a fluid drop, a formal similarity between a drop of height H and a flat layer of the same thickness was used. The relevance of this approximation was justified by a small aspect ratio of lenslike isotropic droplets in FSSFs. It was shown that about six convection cells (rolls) can be formed along the lateral drop dimension. However, the real shape of the drop interface was not taken into account, in spite of the fact that a curvature of the drop interface inevitably imposes a temperature gradient along its free surface.

There is another aspect of the Marangoni convection within ellipsoidal drops which refers to isotropic droplets formed in overheated FSSFs. It is well documented that the surface of the isotropic samples heated above the bulk smectic-isotropic temperature is covered by the smectic layers, the amount of which depends on the degree of overheating [48–50]. The similar situation occurs at the interfaces of isotropic droplets in smectic films. Actually, each droplet is connected with the FSSF of uniform thickness via a meniscus, the profile and height of which are determined by the set of edge dislocation loops located in the film midplane [51,52] [Fig. 1(a)]. In general, a smectic shell covering the drop interface should hinder the development of the Marangoni instability within a fluid drop, the so-called sticking effect. This problem is discussed in more detail below in Sec. II B. This is especially important for isotropic droplets formed in overheated FSSFs, where we deal with the smectic layering at both drop interfaces [Fig 1(a)]. Concerning the lenslike oil drops deposited on FSSFs, their upper surface is directly connected with the air [Fig. 1(b)]. Thus, there are no restrictions for the development of the Marangoni instability in oil drops initiated by the surface tension temperature variations at the upper drop interface. The similar situation with the asymmetric boundary conditions can also be created for the isotropic drops spontaneously formed in FSSFs.

The paper is organized as follows. In Sec. II we present the quantitative description of the equilibrium shape of ellipsoidal drops under study. Section II B is devoted to the description of the thermal stability of the smectic shell covering isotropic droplets and to the analysis of the possibility for thermocapillary motion at the fluid-smectic boundary. The main focus of the remaining sections is a theoretical description of Marangoni flows within the ellipsoidal drop. In Sec. III we present the basic equations and formulate the boundary conditions for ellipsoidal droplets. Section IV contains the main analytical results for Stokes stream functions describing thermocapillary flows in ellipsoidal drops in FSSFs with asymmetric boundary conditions. Section IV E presents the results of numerical simulations of the thermocapillary motion in drops in the frame of numerical experiment. Finally, Sec. V gives a concluding discussion.

II. STATEMENT OF THE PROBLEM AND BASIC EQUATIONS

A. Shape of isotropic droplet in FSSFs

Let us first discuss the shape of the isotropic droplets spontaneously formed in overheated FSSFs. As was indicated earlier, these droplets have the shape of the spherical segments (caps) [Fig. 1(a)] [28,35,37,39]. Due to the prolate shape of the drop the inequality $H \ll R_{\rm cap}$ usually holds (compare with the designations shown in Fig. 1) [53]. The drop is connected with the FSSF via a meniscus the shape of which is determined by its dislocation structure. Initially the surface of the droplet is covered by a certain amount of the smectic layers. The parameters of the spherical segments of the drop are determined from the condition of minimum of its surface energy under assumption that the volume of the droplet is fixed [37]. The minimization is usually made by a Lagrange undetermined multipliers method [37,39] and provides the following relation between the base radius of the cap, $R_{\rm cap}$, and the half-height of the drop, $(H/2)$ [53]:

$$\frac{H}{2} \approx \sqrt{\mathfrak{h}^2 + \frac{\gamma - \gamma_{\rm A}}{\gamma + \gamma_{\rm A}} R_{\rm cap}^2} - \mathfrak{h} \approx \sqrt{\frac{\gamma - \gamma_{\rm A}}{\gamma + \gamma_{\rm A}}}\, R_{\rm cap}, \qquad (1)$$

where $\mathfrak{h}$ is a half of the film thickness, $\mathfrak{h} \ll H$, $R_{\rm cap}$ and γ and $\gamma_{\rm A}$ are the interfacial tensions between the drop-air and the FSSF-air interfaces, respectively. In accordance with the values of the interfacial tensions, the following inequality holds: $H/(2R_{\rm cap}) \ll 1$. The validity of Eq. (1) is confirmed by numerous experimental observations carried out for different smectic materials [28,35,37,38].

In that follows we replace the shape of isotropic droplet in the form of two spherical segments by an ellipsoid (oblate spheroid) characterized by the semiaxes ratio $b/a \ll 1$ (where b and a are a small and large semiaxis of ellipsoid, respectively) (Fig. 2). Doing that we set the b value equal to $H/2$, while the large semiaxis of the ellipsoid attains a value $a = R_b = H\sqrt{1+\xi_0^2}/(2\xi_0)$ (base radius of the ellipsoid drop).

The validity of the above approximation can be justified by equating the volume of isotropic drop in the form of two spherical segments with that of oblate spheroid. Indeed, the volume of an oblate spheroid drop constitutes

$$V_{el} = (4\pi/3)\, a^2\, b = (4\pi/3)\, R_b^2 (H/2). \qquad (2)$$

On the other hand the volume of isotropic drop in the form of two spherical segments can be written as

$$V_{\rm cap} = \pi\,(H/2)\left(R_{\rm cap}^2 + H^2/12\right) + \pi\, 2\,\mathfrak{h}\, R_{\rm cap}^2$$
$$\approx \pi\,(H/2)\, R_{\rm cap}^2 = \pi\,(H/2)\,(R_b + \delta R)^2, \qquad (3)$$

where the difference between $R_{\rm cap}$ and R_b is designated as δR ($(R_{\rm cap} - R_b) = \delta R \ll R_b$). The approximation for $V_{\rm cap}$ in Eq. (3) is valid under assumption $H/(2R_{\rm cap}) \ll 1$. From the equation $V_{el} = V_{\rm cap}$, we obtain the estimate for δR:

$$\delta R \approx 0.15 R_b \ll R_b. \qquad (4)$$

Thus, the above approximation of the lenslike isotropic droplets in FSSF by the oblate spheroid works well due to their small aspect ratio, $H/(2R_{\rm cap}) \ll 1$ (Fig. 3). The small deviations of the ellipsoidal cross section from the initial drop profile can be seen only in the area close to the drop edge.

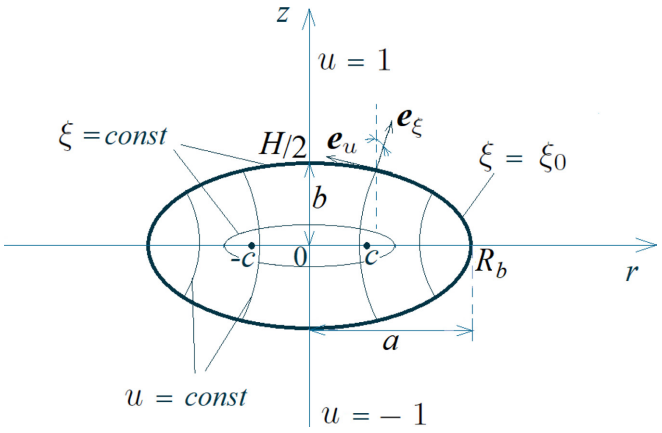

FIG. 2. Representation of the frontal profile of the lenslike isotropic droplet in the approximation of the oblate spheroid. The parameters characterizing the ellipsoidal drop shape are designated in Fig. 1. For convenience, we fixed the zero of the z-coordinate axes in the center of the drop (in the middle plane of the FSSF). The parameters: a, b are the semiaxes of ellipsoid, $a = c\sqrt{1+\xi_0^2} \equiv R_b$, $b = c\,\xi_0 \equiv H/2$, $\xi_0/\sqrt{1+\xi_0^2} = b/a \ll 1$ (the latter inequality is possible only for $\xi_0 \ll 1$), c is a focus distance (coordinate of the focal point). Here $\mathbf{e}_\xi$, $\mathbf{e}_u$ are the unit vectors in the oblate spheroidal coordinates in their meridional plane. Note that $\mathbf{e}_\xi$ is outward normal vector to the oblate spheroidal surface of constant $\xi = \xi_0$, unit vector $\mathbf{e}_\varphi$ is the azimuthal unit vector, oriented beyond the page (sheet) plane, $\mathbf{e}_u$ lies in the tangent plane to the oblate spheroid surface and completes the right-handed basis set $\{\mathbf{e}_u, \mathbf{e}_\xi, \mathbf{e}_\varphi\}$.

We note that the curvature at the end face is much larger than in the upper drop point (their ratio is of the order of a^3/b^3). However, this small area at the drop apex does not affect the general pattern of the convection motion. The same geometrical approach was applied to the lenslike oil drops deposited on FSSFs [Fig. 1(b)]. Contrary to inclusions of the isotropic phase, representing the different phase state of the same liquid crystal material, oil is an individual substance and has the value of surface tension γ_o between the drop-air interface different from that of the isotropic material. Nevertheless, the same Eq. (1) can be used to describe the shape of the oil lenses.

In accordance with the validity of the approximation of the lenslike drops in FSSFs by oblate spheroid, the corresponding conventional orthogonal coordinates u, ξ, φ are consistently employed in further elaborations. Every point of space is described by a triple of numbers (u, ξ, φ), corresponding to a unique point in the Cartesian coordinates (x, y, z). The corresponding orthogonal system of surfaces consists of oblate spheroids formed by surfaces of constant ξ ($\xi = \xi_0$ is the spheroid of the given boundary), one-sheeted hyperboloids of revolution of constant $|u|$ (also known as a circular hyperboloid, the surface generated by a rotation of the hyperbola around the z axis), and planes of φ = const (φ is an azimuthal angle) [54–56] (Fig. 2). The parameter ξ_0 determines the ellipticity ratio, and under the reasonable assumption $\xi_0 \ll 1$ can be written as $\xi_0 = H/(2c) \approx H/(2R_b)$. The above parameters are related to the rectangular coordinates by the following matrix representation [54–56]:

$$\begin{pmatrix} x \\ y \\ z \end{pmatrix} = \begin{pmatrix} c\sqrt{1+\xi^2}\sqrt{1-u^2}\,\cos[\varphi] \\ c\sqrt{1+\xi^2}\sqrt{1-u^2}\,\sin[\varphi] \\ c\,u\,\xi \end{pmatrix}, \tag{5}$$

where the focus distance c plays a role of a scale parameter and

$$-1 \leqslant u \leqslant 1, \quad 0 \leqslant \xi < \infty, \quad 0 < \varphi \leqslant 2\pi. \tag{6}$$

In turn, the representation of the Lame coefficients (metric coefficients) in the above variables reads

$$\begin{aligned} h_u^2 &= \left(\frac{\partial x}{\partial u}\right)^2 + \left(\frac{\partial y}{\partial u}\right)^2 + \left(\frac{\partial z}{\partial u}\right)^2, \\ h_\xi^2 &= \left(\frac{\partial x}{\partial \xi}\right)^2 + \left(\frac{\partial y}{\partial \xi}\right)^2 + \left(\frac{\partial z}{\partial \xi}\right)^2, \\ h_\varphi^2 &= \left(\frac{\partial x}{\partial \varphi}\right)^2 + \left(\frac{\partial y}{\partial \varphi}\right)^2 + \left(\frac{\partial z}{\partial \varphi}\right)^2, \end{aligned} \tag{7}$$

i.e., the metric coefficients are

$$\begin{aligned} h_u &= c\sqrt{\frac{\xi^2+u^2}{1-u^2}}, \quad h_\xi = c\sqrt{\frac{\xi^2+u^2}{1+\xi^2}}, \\ h_\varphi &= c\sqrt{1+\xi^2}\sqrt{1-u^2}. \end{aligned} \tag{8}$$

It is important to note that the values of the parameters u, φ at $\xi = 0$ describe the points ($z = 0$, $r = c\sqrt{1-u^2}$) on the mediated circle disk, for which $\mathbf{r}[\xi = 0, u] = \mathbf{r}[\xi = 0, -u]$, i.e., two points in the oblate spheroid coordinates correspond to a single point in the real physical space. This means that any real physical field must be even function of u at $\xi = 0$. The same is true for a certain set of conditions for the spatial derivatives of the various physical quantities, the velocity, for example, at $\xi = 0$. On the other hand, if the physical field $f[\xi, u]$ splits into a product $f_\xi[\xi] f_u[u]$, then only the single condition appears: the functions $f_\xi[\xi]$ and $f_u[u]$ should have an equal evenness.

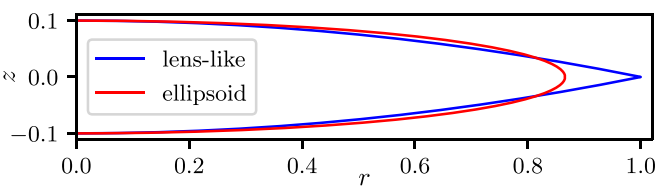

FIG. 3. Illustration of the quality of approximation of the shape of isotropic drop in FSSF by an oblate spheroid.

B. Marangoni instability and the smectic layering at isotropic drop interfaces

As we indicated earlier, the surface of isotropic droplets in FSSFs heated above the bulk smectic-isotropic temperature is covered by a certain amount of smectic layers. In this connection, the natural question arises: what might be the reaction of the smectic layering of the drop on the relatively large positive temperature gradient across it ($T_{up} > T_{dn}$; see Fig. 4). The second question, even more fundamental, is the following: whether the Marangoni instability can develop at the interface between the fluid and the smectic substrate. We remind that smectic state combines a solidlike elasticity along

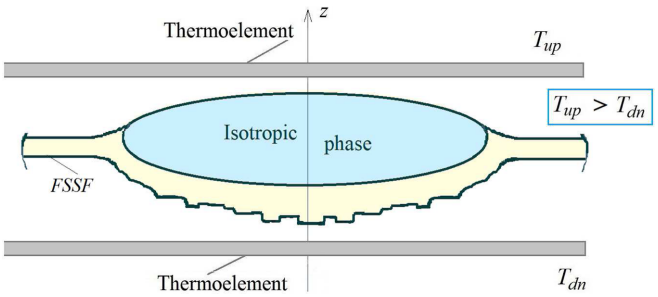

FIG. 4. Sketch of the free-standing smectic film with isotropic drop embedded in it. The upper surface of the droplet is free of the smectic layers, while the lower interface is covered with a nonuniform smectic shell. The thermoelectric devices above and below the drop are used to preset a vertical temperature gradient across the drop, $T_{up} > T_{dn}$.

the layers normal and the liquid behavior in the plane of layers, an absence of the resistance for an applied shear stress [57]. The second question applies equally to isotropic droplets formed in an overheated FSSF and to oil lenses deposited on it [Fig. 1(b)].

Let us start with the stability of the smectic layering. The amount of smectic layers on the surface of isotropic droplet in FSSFs depends on the degree of overheating, initial film thickness, energetics and probability of defect formation, etc. [51,52]. As in any layered structure, discrete change of the amount of smectic layers in the film can proceed only by thermal generation of elementary edge dislocation loops [46,58]. This usually occurs in the middle plane of the film and corresponds to the formation either of the surface depletion areas (holes) or the surface bulge areas (islands). The dislocation loops of the critical radius can be generated stochastically in the film under favorable conditions, and then they are growing at certain rate either in the direction of the meniscus producing thinner films, or in the opposite direction, film thickening [31,52,59–61].

The general approach allowing one to calculate the frequency of thermal generation of any type of critical nucleus of energetically favorable defects was proposed by Langer and Fisher [62,64]. According to our previous findings [52,65], the typical value of critical work W_c for nucleation of dislocation loop of critical radius $\sim 10^{-8}$–10^{-7} m in the middle plane of overheated smectic film is of the order $W_c \sim 10^{-20}$ J. This is smaller than the threshold energy $W_c^* = 2.5 \times 10^{-19}$ J, thus indicating that if the temperature of the upper drop surface is sufficiently higher than that at the bottom interface, a large number of dislocation loops appears leading to the thinning of the upper smectic shell of the drop. The role of the heating protocol (the rate and the waiting period) is essential for the thinning of the smectic layering to proceed. Applying the slow preliminary heating [51] it is possible to generate one dislocation loop after another in the smectic shell on the top of a drop, and in such layer by layer fashion move away the smectic layers from the hot half of the drop (see also [66]).

The situation at the bottom side of the drop is different. In the presence of the positive temperature gradient ($T_{up} > T_{dn}$) the temperature of the meniscus connecting the isotropic drop with FSSF is higher than that at the bottom side of the drop. For relatively large temperature difference the energy gain associated with nucleation and growth of dislocation loops of excess smectic layers becomes energetically favorable [52]. The material necessary for the smectic shell at the bottom side of the film to thicken flows from the meniscus surrounding the isotropic drop, thus producing the sequence of islands (bulge areas in the shell) (Fig. 4). This corresponds to the disappearance of the whole set of dislocation loops from the meniscus. At a certain stage of this process, the activation energy for the formation of such dislocation loops becomes larger than the threshold energy, and the process of formation of islands at the bottom shell of the drop terminates. The similar behavior related to the formation and movement of islands on the surface of smectic bubble subjected to a temperature gradient was observed in microgravity experiments on the International Space Station [43].

Now, we turn to the analysis of the possibility of Marangoni convection in the fluid, which is bounded by a smectic shell (substrate). This configuration applies equally to isotropic droplets formed in overheated FSSFs and to oil lenses embedded in FSSFs (Figs. 1 and 4). The Marangoni forces act tangentially at the curved fluid-smectic interface, thus inducing the axially symmetric flow of a smectic material in the plane of smectic layers from the meniscus (hot area) downwards in the direction of the bottom point of the smectic shell (cold area). These fluid motions interfere with each other in the bottom area of the smectic shell, thus producing smectic islands and steps in the film. As a consequence of this process, the lamellar structure in the smectic film is strongly destructured in this area, producing the domains in which the orientation of the layer normals is inclined relative to the initial fluid-smectic interface. This situation is somewhat similar to a process of collapse of a smectic bubble inflated at the end of a capillary tube [67]. In both cases the lamellar structure in the area close to the meniscus is strongly destroyed. Below we show that in this case the tangential component of the smectic elastic force compensates the Marangoni forces at the fluid-smectic interface, thus terminating the flow of the smectic material. This means that at the border between the smectic and fluid its tangential velocity turns to zero, which corresponds to the sticking (no-slip) condition.

Indeed, in the invariant form the smectic elastic tensor can be written as (see, for example, [45,68])

$$\sigma_{ik}^{(el)} = B\,(\nabla_n u_{sm}) n_i n_k, \tag{9}$$

where B is the smectic elastic modulus, corresponding to compression (dilatation) of the smectic layers, u_{sm} is the displacement field of the smectic layers, $\mathbf{n}$ is the normal to the surface of smectic domains, $(\nabla_n u_{sm}) = (\mathbf{n}\nabla u_{sm})$. The k component of the force $\mathbf{f}$, acting on the bottom (internal) drop interface reads

$$f_k = B\,(\nabla_n u_{sm})\,(\mathbf{l}\,\mathbf{n})\,n_k - \delta p\, l_k, \tag{10}$$

where δp is the pressure difference, $\mathbf{l}$ is the normal to the bottom interface, and $(\mathbf{l}\,\mathbf{n})$ is their scalar product. Using the condition of balance of the normal forces at the internal interface between the smectic and fluid

$$B\,(\nabla_n u_{sm})\,(\mathbf{l}\,\mathbf{n})\,n_k l_k - \delta p\, l_k l_k = 0, \tag{11}$$

one can obtain the pressure difference acting at the interface

$$\delta p = B\,(\nabla_n u_{sm})\,(\mathbf{l}\,\mathbf{n})^2. \tag{12}$$

After substitution of the expression for δp into Eq. (10) the condition of equilibrium of the tangential forces takes the form

$$B\,(\nabla_n u_{sm})\,(\mathbf{l}\,\mathbf{n})\,(\mathbf{n}\,\mathbf{m}) - \delta p\,(\mathbf{l}\,\mathbf{m}) = B\,(\nabla_n u_{sm})\,(\mathbf{l}\,\mathbf{n})\,(\mathbf{n}\,\mathbf{m}), \tag{13}$$

where $\mathbf{m}$ is the unit vector, tangent to the internal interface ($(\mathbf{l}\,\mathbf{m}) = 0$). Thus, the projection of the force $\mathbf{f}$ on the unit vector $\mathbf{m}$ is able to compensate the Marangoni tangential force, that corresponds to the condition of sticking of the fluid at this interface.

In that follows we consider the situation, when the top of the drop is free from the smectic layers, i.e., it has the free boundary, while the bottom half of the drop is in contact with the static smectic substrate (compare with [43]). This asymmetric geometry applies equally to isotropic drops formed in an overheated FSSF and to oil lenses embedded in it.

III. GOVERNING EQUATIONS AND BOUNDARY CONDITIONS

Normally, surface tension of a liquid is a decreasing function of temperature

$$\gamma = \gamma_0 - \varsigma\, T', \tag{14}$$

where $T' = (T_{dr} - \bar{T})$, T_{dr} is a current drop temperature, $\bar{T}$ is some constant temperature (far from the drop at $z = 0$), and ς is the tension temperature coefficient ($\varsigma > 0$). Below we omit the prime symbol for simplification of the further derivations. We recall that only for the sufficient temperature gradient across the flat fluid film, the small temperature variations along the surface initiate change of the surface tension, which in turn cause the fluid to flow and thereby tend to maintain the initial temperature disturbances. Because of viscosity of the liquid the moving surface gives rise to a shear stress, which drives a flow in the film interior [4,8,9]. As a result the flat fluid film loses its mechanical stability and the Marangoni convective patterns are developed, as have been shown theoretically by Pearson [69] using the linear instability analysis.

In this work we present a quantitative description of the Marangoni flows in ellipsoidal isotropic droplets formed in FSSFs based on the formalism of the Stokes stream functions. Contrary to the flat fluid films, the mechanical equilibrium within such drops is absent due to their curved shape. Because of the nonuniform temperature distribution the tangential thermocapillary force always exists at the free drop surface (Marangoni force). This leads to a fluid flow along its curved interface, making the thermocapillary flow within the drop thresholdless.

Consider the horizontal FSSF with the fluid isotropic droplets in it, which is placed between two thermoelectric devices. The film is parallel to the x-y plane, with the layer normal directed along the z axis. The origin of the coordinate frame along z is taken in the center of the drop. The construction of setup allows the heat transfer from the hot plate to the cold plate placed at the bottom side of the drop. This corresponds to the positive direction of the temperature gradient $\partial T/\partial z\,(T_{dn} < T_{up})$ (Fig. 4) and ensures the absence of the Rayleigh convection in the surrounding air.

The flow is governed by set of equations, namely, the Navier-Stokes equation, the thermal energy transport equation, the continuity equation for the incompressible fluid, and the equation for thermal conduction in the surrounding air [from (15) to (18)] [5,8,9,70,73]:

$$\frac{\partial \mathbf{v}}{\partial t} = -\frac{1}{\rho_0}\,(\nabla p) + \nu\,\nabla^2 \mathbf{v} - \beta\, T\, g\, \mathbf{e}_z, \tag{15}$$

$$\frac{\partial T}{\partial t} + (\mathbf{v}\,\nabla)\,T = \chi\,\Delta T, \tag{16}$$

$$(\nabla\,\mathbf{v}) = 0, \tag{17}$$

$$\frac{\partial T_a}{\partial t} = \chi_{\text{air}}\,\Delta T_a, \tag{18}$$

which correspond to the Boussinesq approximation (i.e., $|\alpha\, p| \ll |\beta\, T| \ll 1$, where t is the time, $T = T_0 + T_1$, and pressure $\mathcal{P} = p_0 + p$, $\nabla p_0 = \rho_0 \mathbf{g}$, $\mathbf{g}$ is gravitational acceleration). $T_a = (T_{\text{air}} - \bar{T})$, T_{air} is a current temperature in the surrounding air. In above equations β and α are the coefficients of thermal expansion and isothermal compressibility, respectively, $\rho_0 = \rho[\bar{\mathcal{P}}, \bar{T}]$ is some constant density of fluid, $\nu = \eta/\rho_0$ is the kinematic viscosity, η is a dynamical viscosity coefficient, and $\mathbf{v}$ is the flow velocity. The coefficient of temperature conductivity is designated as $\chi = \varkappa\,(\rho_0 c_p)^{-1}$, where $\varkappa$ is the thermal conductivity, c_p is a specific heat. In above equations the quadratic over perturbations inertial terms were omitted. Below we apply a conventional linear perturbation theory to describe the small deviations of the solutions in the considered system from the zero stationary approximation, where $\partial T_0/\partial z = A > 0$, $|T_1| \ll T_0$ [8,70].

The term $-\beta\, T\, g\, \mathbf{e}_z$ in Eq. (15) corresponds to the convective buoyancy force in the drop. Bearing in mind that Marangoni convection at small length scales (i.e., in small size drops we deal with) prevails over the buoyant convection, we can neglect this term in Navier-Stokes equation in comparison with the viscous term due to the small Rayleigh number $R = g\beta\, A\, H^4/(\nu\,\chi)$ [8]. The relative role of two types of convection can be evaluated from the comparison of the Rayleigh and Marangoni

$$\text{Ma} = \frac{\varsigma H^2 A}{\chi\,\eta} \tag{19}$$

numbers [8]; therefore, the Marangoni convection is dominating at drop heights

$$H \ll H_c = \sqrt{\frac{\varsigma}{\rho\, g\beta}} \sim 10^4\ \mu\text{m}, \tag{20}$$

where the typical values of the liquid crystal parameters [72] are used. For the ordinary fluids the transition to buoyancy-dominated convection occurs around a 1 cm, which is many orders of magnitude larger than the droplets size considered in our theory [8,45,70]. Thus, in our case we deal with the pure Marangoni convection initiated by the gradients of the surface tension at the drop interfaces.

At this point it is relevant to summarize the main assumptions made to develop the presented analytical model:.

$$\mathfrak{h} \ll \frac{H}{2} \ll R_{\rm cap} \rightarrow \xi_0 \ll 1, \tag{21}$$

$$\varsigma > 0, \tag{22}$$

$$|\alpha\, p| \ll |\beta\, T_1| \ll 1, \tag{23}$$

$$|T_1| \ll T_0, \tag{24}$$

$$\mathrm{Ma} \gg R, \tag{25}$$

$$\delta\gamma/\gamma \ll 1. \tag{26}$$

The condition (21) indicates that highly anisometric oblate spheroids should be considered within our model. As regards the inequalities (23) and (24), they correspond to the fulfillment of the Boussinesq approximation. The condition (25) is fulfilled in view of Eq. (20).

Because all the coefficients in Eqs. (15)–18) are not dependent on time, we can find the stationary solutions of our thermocapillary problem. In this case the left parts of Eqs. (15)–(18), containing terms with the time derivatives, vanish. Equations (15)–(18) are written in a general view with conjunction to the conventional rectangular coordinate z. To solve the problem of Marangoni convection in ellipsoidal fluid drops it is convenient to rewrite all governing Eqs. (15)–(18) and boundary conditions using the orthogonal oblate spheroid coordinates (see Sec. II A and Fig. 2).

Let us start with the formulation of the boundary conditions for our problem. At the surface of the oblate spheroidal drop ($\xi = \xi_0$) the boundary conditions for the fluid velocity components can be written as

$$v_\xi = 0 \ \ (\mathrm{at}\, \xi = \xi_0), \tag{27}$$

that is, the condition of an absence of flow of the material through the boundary surface of the drop; additionally

$$v_u = 0 \quad (\mathrm{at}\, \xi = \xi_0,\ u \in [-1, u_0]), \tag{28}$$

which determines the condition of sticking of a fluid at the bottom boundary surface of the drop (in a contact with the smectic shell). The value of u_0 determines an extension of the boundary with the no-slip condition along the drop interface: $u = 0$ corresponds to its termination at the circular edges of the drop, while the positive u indicates the partial overlap of the upper drop interface by the region with the sticking conditions. The later is due to a presence of the meniscus connecting the drop with the FSSF (see Figs. 1 and 4). Next, we turn to the boundary conditions for the temperature deviations and the heat fluxes

$$T_a|_{\xi=\xi_0} = T|_{\xi=\xi_0}, \tag{29}$$

$$T_a|_{\xi\rightarrow\infty} = C_{\rm air}\, c\, u\, \xi\,, \tag{30}$$

$$\varkappa \frac{1}{h_\xi} \frac{\partial T}{\partial \xi}\bigg|_{\xi=\xi_0} = \varkappa_{\rm air} \frac{1}{h_\xi} \frac{\partial T_a}{\partial \xi}\bigg|_{\xi=\xi_0}, \tag{31}$$

that are the boundary conditions of the equality of the temperature deviations and the normal heat flux at the air-drop interface. It is important that for the system under consideration $\varkappa = \varkappa_{\rm fluid} \simeq 0.25\ \mathrm{W(m\ K)^{-1}} \gg \varkappa_{\rm air} \simeq 0.026\ \mathrm{W(m\ K)^{-1}}$ [41], which means an almost instant thermal flow inside the drop comparatively to the surrounding air.

Another class of the boundary conditions for our problem corresponds to a stress balance at the surface of the droplet projected both in the normal and tangential directions. The boundary condition for the balance of tangential viscous and Marangoni ($G_{\rm Ma}$) forces on the free top boundary of the ellipsoidal drop is given by the expressions

$$\sigma_{u\xi} e_\xi = \eta\left(\frac{\partial_u v_\xi}{h_u} + \frac{\partial_\xi v_u}{h_\xi} - \frac{v_u}{h_\xi}\frac{\xi}{\xi^2+u^2}\right)$$
$$= G_{\rm Ma} = \frac{\partial_u \gamma}{h_u} \quad (\mathrm{at}\, \xi = \xi_0,\ u \in [u_0, 1]), \tag{32}$$

$$\sigma^{\varphi\xi} = 0, \tag{33}$$

obtained by substitution of the variables ξ, u to Eqs. (A7) and (A8) (see Appendix A). Equation (32) reflects the nonuniformity of the surface tension γ at the upper drop surface, thus introducing the thermocapillary force, which drives the convection process [70]. At this point it is appropriate to note that the zero approximation of the system of Eqs. (15)–(18) coincides with the zero approximation over the temperature coefficient of surface tension ς [i.e., when $\varsigma = 0$; see Eq. (14)]. The detail analysis of these boundary conditions is given in Appendix A.

As to the normal stress balance, it is replaced in our case by the assumption that the ellipsoidal form of a droplet practically does not change in the process of convection (compare with [24]). This assumption is valid because the pressure deviation due to the nonhomogeneity of the temperature across the drop boundary is negligibly small: $\delta p/p \sim \delta\gamma/\gamma \sim 10^{-4}$–$10^{-3} \ll 1$ (see [66,72]), in accordance with Eq. (26).

It is convenient to solve the hydrodynamic equations of Marangoni convection for the axially symmetric ellipsoidal drops in terms of 2D Stokes stream functions $\psi[u,\xi]$ [56]. By definition, this function determines the instant fluid flow rate divided by 2π (the half of the total spatial angle). The stream function ψ is scaled by $\chi c^2/H$, and thus used in the dimensionless form below. According to [56], the velocity field is related to the stream function by the following equation written in oblate spheroidal coordinates

$$\mathbf{v} = \frac{1}{h_\varphi}[\mathbf{e}_\varphi \times \nabla\psi]. \tag{34}$$

After substitution of Eq. (8) into Eq. (34) one obtains

$$\mathbf{v} = -\frac{\mathbf{e}_u}{h_\xi h_\varphi}\partial_\xi\psi + \frac{\mathbf{e}_\xi}{h_u h_\varphi}\partial_u\psi, \tag{35}$$

where $\mathbf{e}_\xi$ and $\mathbf{e}_u$ are the unit vectors along ξ and u axes, respectively.

To obtain the dynamic equation for the Stokes stream function it is convenient to introduce the vorticity

$$\vec{\varpi} = [\nabla \times \mathbf{v}]. \tag{36}$$

After substitution of Eqs. (35) to (36) one arrives at

$$\vec{\varpi} = \frac{\mathbf{e}_\varphi}{h_\varphi}\hat{\mathrm{E}}^2\psi, \tag{37}$$

where

$$\hat{E}^2\psi = \frac{1}{c^2\,(u^2+\xi^2)}\left[(1+\xi^2)\,\frac{\partial^2\psi}{\partial\xi^2} + (1-u^2)\,\frac{\partial^2\psi}{\partial u^2}\right]. \quad (38)$$

Then, applying the rotor operation to the vorticity $\vec{\varpi}$ twice, one obtains

$$[\nabla \times [\nabla \times \vec{\varpi}]] = -\frac{\mathbf{e}_\varphi}{h_\varphi}\hat{E}^2\,(\hat{E}^2\,\psi) = -\frac{\mathbf{e}_\varphi}{h_\varphi}\hat{E}^4\psi. \quad (39)$$

Applying the rotor operation to both sides of Eq. (15), one excludes the pressure p, and using the continuity equation (17), Eqs. (36), (37), and (39), and taking the equality $[\nabla \times \nabla^2\mathbf{v}] = -[\nabla \times [\nabla \times \vec{\varpi}]]$ into account, expresses the resulting equation through the single variable ψ [56]. The convective buoyancy force in Eq. (15) was disregarded, as we argued above. In such a way the Navier-Stokes equation in the Boussinesq approximation (15) for the stationary regime is replaced by the following equation for the stream function:

$$\hat{E}^2\,(\hat{E}^2\,\psi) = 0. \quad (40)$$

We note that the boundary condition represented by Eq. (27) with account to Eq. (35) takes the form

$$\psi[\xi_0, u] = 0. \quad (41)$$

It is important to check the obtained solutions on the absence of singularities; see Sec. II A. In the first place this applies to the components of the velocity field v_x, v_z and the vorticity $\vec{\varpi}$, which should be continuously differentiable functions.

IV. RESULTS

A. Stokes stream functions and velocity fields

In this section we generalize the formalism developed by Happel and Brenner [56] to solve Eq. (40) for the stream function ψ . In doing so we first obtain the solutions of equation $\hat{E}^2\,\psi = 0$. According to definition of the stream function, $\psi = 0$ along the z axis, i.e., for $u = 1$ or $u = -1$. The solutions for ψ can be either symmetrical, or asymmetrical with respect to the variable u. This means that all solutions of Eq. (40) should be proportional either to $(1-u^2)$, or to $u\,(1-u^2)$, respectively. In turn, in accordance with the properties of the Legendre polynomials, $P_n[u]$, the solutions of the equation $\hat{E}^2\,\psi = 0$ are proportional to the integrals from the Legendre polynomials [see Appendix B, where the straight method of derivation of the solutions of Eq. (40) is presented]. This allowed us to obtain the full set (the linear space) of solutions of Eq. (40), satisfying all of the above mentioned requirements.

However, the above mentioned straight method of derivation of the solutions of Eq. (40) is too complicated, especially if we extend it for the large number of the accounted basic functions. We note that the full solution for the stream function represents the sum over the limited amount of the basic functions $\{\psi_n[\xi, u]\}$, which is determined by the number N_r. Instead that, we developed the operator method of the solution of Eq. (40) based on the introduction of a set of the recursive operators, and the special algebraic technique which allows the stream functions of different order to interconnect with each other (see Appendixes C, D, and E). The general

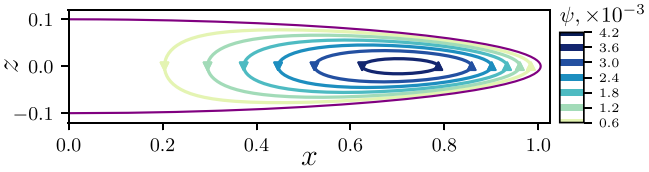

FIG. 5. Streamlines corresponding to the basic stream function ψ_3 for $\xi_0 = 0.1$; the ξ_0 value determines the ellipticity ratio of the droplet and is equal to $H/(2c) \approx H/(2R_b)$ (see Sec. II A). All lengths are shown in the dimensionless form.

expression for the n-th basic stream function ψ_n can be written as

$$\psi_n[\xi, u] = \mathcal{F}_n\left(\mathcal{X}_{n-2}^{(1)} - \frac{\mathcal{X}_{n-2}^{(1)}[\xi_0]}{\mathcal{X}_n^{(1)}[\xi_0]}\mathcal{X}_n^{(1)}\right) + \mathcal{F}_{n-2}\left(\mathcal{X}_n^{(1)} - \frac{\mathcal{X}_n^{(1)}[\xi_0]}{\mathcal{X}_{n-2}^{(1)}[\xi_0]}\mathcal{X}_{n-2}^{(1)}\right), \quad (42)$$

where the function

$$\mathcal{F}_n[u] = \int_{-1}^{u} P_n[u']\,du' = \frac{P_{n+1}[u] - P_{n-1}[u]}{2n+1} \quad (43)$$

is expressed via the Legendre polynomials $P_n[u]$ of the order n, and

$$\mathcal{X}_n^{(1)}[\xi] = \frac{\Xi_{n+1}^{(1)}[\xi] - \Xi_{n-1}^{(1)}[\xi])}{2n+1}, \quad (44)$$

where $\Xi_n^{(1)}[\xi]$ is the solution of Eq. (C2), i.e., $\Xi_n^{(1)}[\xi]$ is the ξ-dependent function multiplier in the solution of the Laplace equation $\Delta\phi_n = 0$ in the ellipsoidal coordinates (see Appendixes C, D, and E). The above formalism is applied for $n > 2$. The streamlines for the first four stream functions ψ_n, corresponding to ellipticity ratios $\xi_0 = 0.1$, $\xi_0 = 0.2$, are presented in Figs. 5–8. The lengths x and z are shown in the dimensionless form, being scaled by $c = \frac{H/2}{\xi_0} = a\,(\sqrt{1+\xi_0^2})^{-1}$. The number of vortices along the long drop semiaxis a for each ψ_n increases with the increase of n. It is readily seen that with increasing of the ellipticity ratio ξ_0 the flow pattern remains the same, only the scale is changed. The basic stream functions described by Eq. (42) satisfy the symmetry of the problem and the condition of the absence of fluid flow through the external drop boundary (see Sec. III).

Provided that the stream functions describing the thermocapillary motion are known, the velocity components, satisfying the corresponding boundary conditions (28) and

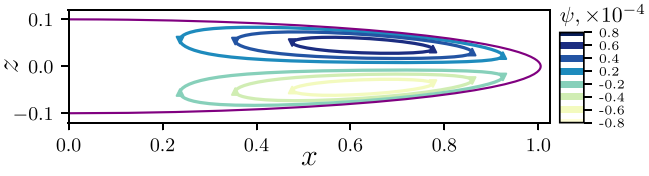

FIG. 6. Streamlines corresponding to the basic stream function ψ_4 for $\xi_0 = 0.1$.

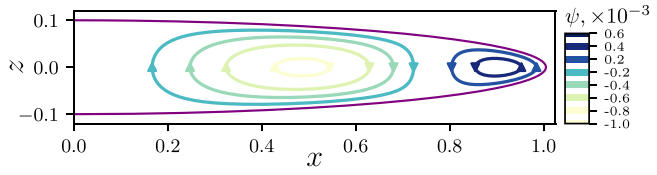

FIG. 7. Streamlines corresponding to the basic stream function ψ_5 for $\xi_0 = 0.1$.

(32), can be obtained:

$$v_\xi[\xi, u] = \frac{1}{c^2(\sqrt{1+\xi^2}\sqrt{u^2+\xi^2})}\frac{\partial\psi[\xi,u]}{\partial u},$$
$$v_u[\xi, u] = -\frac{1}{(c^2\sqrt{1-u^2}\sqrt{u^2+\xi^2})}\frac{\partial\psi[\xi,u]}{\partial\xi}. \quad (45)$$

In turn, the velocity components v_x, v_z in oblate spheroid coordinates in accordance with Eqs. (A3)–(A6) appear as

$$v_x[\xi, u] = \frac{1}{\sqrt{u^2+\xi^2}}(\xi\sqrt{1-u^2}\,v_\xi - u\sqrt{1+\xi^2}\,v_u)\cos\varphi, \quad (46)$$

$$v_z[\xi, u] = \frac{1}{(u^2+\xi^2)^{1/2}}(u\sqrt{1+\xi^2}\,v_\xi + \xi\sqrt{1-u^2}\,v_u). \quad (47)$$

Next, we aim to derive the basic set of the stream functions $\{\psi_{j,st}\}$, explicitly describing the convection flow for the asymmetric boundary conditions, i.e., for the case of fluid sticking at the bottom drop surface: $\partial_\xi\psi_{j,st}[\xi = \xi_0] = 0$ for $u \in (-1, 0)$ (i.e., for $u_0 = 0$), with designation $\ldots_{st}$ indicating this configuration. To solve this problem it is optimal to represent the set of basic stream functions $\{\psi_j[\xi, u]\}$ [see Eq. (43)] and corresponding tangential velocities $v_{u,j}$ as sets of odd and even functions. This allows us to obtain the correct view of the new basic stream functions, satisfying the nonsymmetric boundary conditions. Moreover, these stream functions provide a continuous variation through the points of contact between the free and bounded by the smectic layers surfaces of the drop (for details of the calculation procedure see Appendix F). The streamlines corresponding to the three first stream functions $\psi_{j,st}[\xi, u]$, satisfying the boundary conditions of sticking at the bottom interface, are shown in Figs. 9–12. The number of vortices along the long drop semiaxis a for each $\psi_{j,st}$ is equal to j. The above solutions were

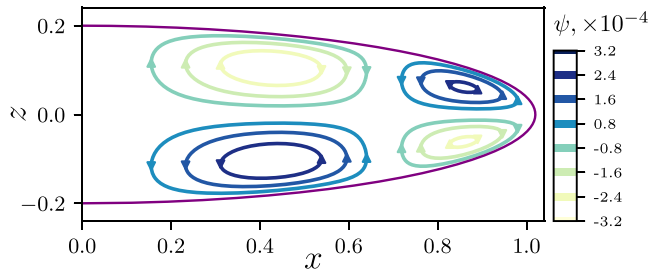

FIG. 8. Streamlines corresponding to the basic stream function ψ_6 for $\xi_0 = 0.2$.

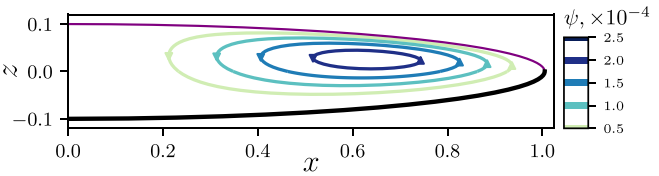

FIG. 9. Streamlines corresponding to the first stream function $\psi_{1,st}$, for $\xi_0 = 0.1$. The bold black line at the bottom part of the drop indicates that the sticking (no slip) conditions are fulfilled at this interface. The same symbol will be used in the following figures. In contrast to this, the upper part of the drop is free (in contact with the air).

obtained for the case of the strongly oblate spheroid, which is in accordance with the condition $\xi_0 \ll 1$ (21).

The comparative analysis of the solutions for the basic stream functions for the cases of the free drop surface $\{\psi_n\}$, and for the asymmetric boundary conditions $\{\psi_{j,st}\}$, indicates the essentially different character of the corresponding convection patterns (Figs. 5–8 and 9–12). For the case of the drop with the free surface the thermocapillary convection with two rows of vortices (top and bottom) is principally possible under certain parameters of the problem (for example, for a large temperature gradient across the drop). Contrary to this, for the drops with the sticking boundary conditions at the bottom drop interface, such a regime is forbidden because there is no driving Marangony tangential force at the boundary with smectic. Only the single row of convection patterns is observed in this case (see Figs. 9–12). Moreover, in this case a thin boundary region is formed close to the bottom drop interface, where the flow is absent. Another interesting observation is that in dependence on the parameters of the problem the convection regimes with the different number of vortices along the direction of the axial drop cross section can be realized.

B. Temperature distribution

Now we can turn to the couple of governing equations of Marangoni convection within ellipsoidal fluid drops describing the thermal energy transport inside the drop and the thermal conduction in the surrounding air [Eqs. (16) and (18)]. We need to know the temperature distribution to obtain the general stationary solution of the thermocapillary convection inside the drop. The conventional linear perturbation theory is applied again to solve the system of Eqs. (15)–(18) in the stationary regime. In doing so the approximations $T = T_0 + T_1$ and $T_a = T_{0\,\mathrm{air}} + T_{1\,\mathrm{air}}$ are used, where T_0 is the solution for the case, the fluid motion is absent, and T_1 is the small

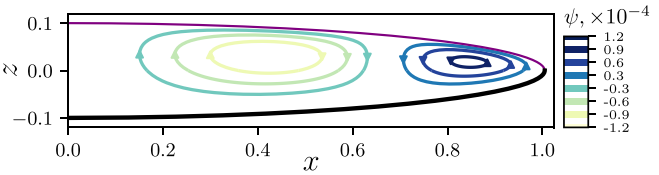

FIG. 10. Streamlines corresponding to the first stream function $\psi_{2,st}$, for $\xi_0 = 0.1$.

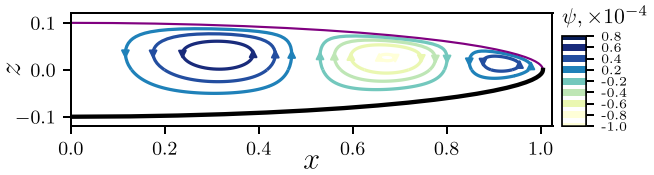

FIG. 11. Streamlines corresponding to the first stream function $\psi_{3,st}$, for $\xi_0 = 0.1$.

temperature deviation. This results in the following equations for the temperature deviations:

$$\Delta T_0 = 0, \tag{48}$$

$$\Delta T_{0\,\mathrm{air}} = 0, \tag{49}$$

$$\chi\,\Delta T_1 = v_z \partial_z T_0, \tag{50}$$

$$\Delta T_{1\,\mathrm{air}} = 0. \tag{51}$$

The full set of solutions of the above Laplace equations in oblate spheroid coordinates is given in Appendix C. As a first step we calculate the temperature distribution T_0. In accordance with the symmetry of the problem the stationary heat flux far away from the drop (in the surrounding air) is directed along the z axis: $T_{0\,\mathrm{air}} \to C_{\mathrm{air}}\, c\, u\, \xi$, where C_{air} is a uniform temperature gradient across the air, $z = c\, u\, \xi$. According to Appendix C the regular kernel of the Laplace operator can be expressed as $P_n[u]\,\Xi_n^{(1)}[\xi]$. The corresponding heat flow is regular at the point $u = \xi = 0$. To find the temperature distribution in the air it is convenient to use the linear combinations of $\Xi_n^{(1,2)}$, damped at $\xi \to +\infty$, which are designated below as $\Xi_n^{(a)}$. Thus, the solution in the air has the form

$$T_{0\,air} = C_{\mathrm{air}}\, c\, \underbrace{u\,\xi}_{P_1\,\Xi_1^{(1)}} + \sum_{n=1}^{\infty} \alpha_n\, P_n[u]\, \Xi_n^{(a)}[\xi]. \tag{52}$$

The temperature distribution T_0 inside the drop can be written (with account for the regularity condition of the heat flow at the point $u = \xi = 0$) as

$$T_0 = \sum_{n=1}^{\infty} \beta_n P_n[u]\,\Xi_n^{(1)}[\xi]. \tag{53}$$

The solutions of Eqs. (52) and (53) should satisfy the boundary conditions (29) and (31) at $\xi = \xi_0$; since Legendre's polynomials $\{P_n\}$ form an orthogonal basis, these conditions

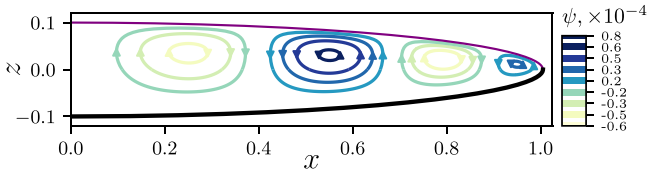

FIG. 12. Streamlines corresponding to the first stream function $\psi_{4,st}$, for $\xi_0 = 0.1$.

have to hold for any value of the variable u:

$$n = 1: \begin{cases} \beta_1 \xi_0 = C_{\mathrm{air}}\, \xi_0 + \alpha_1\, \Xi_1^{(a)}\big|_{\xi=\xi_0}, \\ \varkappa\, \beta_1 = \varkappa_{\mathrm{air}}\, C_{\mathrm{air}}\, c + \varkappa_{\mathrm{air}}\, \alpha_1\, \partial_\xi\, \Xi_1^{(a)}\big|_{\xi=\xi_0}, \end{cases} \to$$

$$\to \beta_1 = c\, \underbrace{C_{\mathrm{air}}\, \kappa\, \frac{1 - \xi_0 \big(\ln \Xi_1^{(a)}\big)'\big|_{\xi=\xi_0}}{1 - \kappa \xi_0 \big(\ln \Xi_1^{(a)}\big)'\big|_{\xi=\xi_0}}}_{A} = c\, A, \tag{54}$$

$$\alpha_1 = -C_{\mathrm{air}}\, \frac{(1-\kappa)}{\big(\Xi_1^{(a)}/\xi_0 - \kappa\, \partial_\xi\, \Xi_1^{(a)}\big)\big|_{\xi=\xi_0}}, \tag{55}$$

where $\kappa = \varkappa_{\mathrm{air}}/\varkappa$ is a relative heat conductivity.

$$n > 1: \begin{cases} \beta_n \xi_0\, \Xi_n^{(1)}\big|_{\xi=\xi_0} = \alpha_n\, \Xi_n^{(a)}\big|_{\xi=\xi_0}, \\ \varkappa\, \beta_n\, \partial_\xi\, \Xi_n^{(1)}\big|_{\xi=\xi_0} = \varkappa_{\mathrm{air}}\, \alpha_n\, \partial_\xi\, \Xi_n^{(a)}\big|_{\xi=\xi_0}, \end{cases} \to$$

$$\to \beta_n = 0, \alpha_n = 0 \quad \text{for n} > 1.$$

In that follows we present all the variables in dimensionless form, using appropriate scaling relations, symbol $\widetilde{...}$ designates the dimensionless variables, correspondingly. All lengths are scaled by $c = \frac{H/2}{\xi_0} = \frac{a}{\sqrt{1+\xi_0^2}}$, velocities by χ/H (i.e., $\mathbf{v} = \tilde{\mathbf{v}}\,\chi/H$), time by $c/v = \frac{H^2/2}{\xi_0\,\chi}$, and temperatures by HA (i.e., $T = \tilde{T}\,A\,H$) [2,8]. Then for the dimensionless temperature distribution $\widetilde{T}_0$ we obtain

$$\widetilde{T}_0 = \frac{u\xi}{2\xi_0}. \tag{56}$$

Let us stress that the derivation of the temperature distribution $\widetilde{T}_0$ is necessary to find the solution for the stream functions describing the main contribution to the stationary thermocapillary convection within the drop.

In turn, the dimensionless equation for the temperature distribution $\widetilde{T}_1$ reads

$$\widetilde{\Delta}\widetilde{T}_1 = \frac{c^2}{H^2}\,\widetilde{v}_z = \frac{1}{4\xi_0^2}\,\widetilde{v}_z. \tag{57}$$

Below we omit the symbol $\widetilde{...}$ for simplicity.

It is convenient to rewrite Eq. (57) for the distribution of the temperature deviation T_1 inside the drop in terms of the stream function ψ:

$$[\partial_\xi (1+\xi^2)\partial_\xi + \partial_u (1-u^2)\partial_u]\, T_1 = \frac{(u\partial_u\psi - \xi\,\partial_\xi\psi)}{4\xi_0^2}. \tag{58}$$

The right side of Eq. (58) can be decomposed over the Legendre's polynomials in the form $\sum_n f_n[\xi]P_n[u]$. In such a way we can find the temperature response to each $f_n[\xi]P_n[u]$ in view of $T_n[\xi]P_n[u]$. Thus, for each functional coefficient $T_n(\xi)$ we obtain the following equation:

$$\partial_\xi (1+\xi^2)\partial_\xi T_n - n(n+1)T_n = f_n[\xi]. \tag{59}$$

It is easy to check that the right part of Eq. (59) can be presented as a linear combination $f_n = \sum_k \mathcal{W}_{n,k}^{(1)}\,\Xi_k^{(1)}$, where $\mathcal{W}_{n,k}^{(1)}$ is the expansion coefficient. This allows us to write the

response of the functional coefficient $T_n(\xi)$ to each Ξ_k as

$$T_{n,k}[\xi] = \underbrace{\frac{\mathcal{W}^{(1)}_{n,k}}{k(k+1)-n(n+1)}}_{W^{(1)}_{n,k}} \Xi^{(1)}_k[\xi], \quad n \neq k. \tag{60}$$

The condition $n \neq k$ is always valid here due to the specific form of the expression for the velocity component v_z (see Appendix F).

To derive the full solution for the temperature deviations T_1 within the drop it is necessary to add to a partial solution $\sum_k W^{(1)}_{n,k}\, \Xi^{(1)}_k[\xi]$ of Eq. (58) the homogeneous solution $\Lambda^{(1)}_n \Xi^{(1)}_n[\xi]$:

$$T_1 = \sum_n \left\{ \sum_k W^{(1)}_{n,k}\, \Xi^{(1)}_k[\xi] + \Lambda^{(1)}_n\, \Xi^{(1)}_n[\xi] \right\} P_n[u]. \tag{61}$$

In the next step it is necessary to take into account the continuity of heat and the heat flux at the boundary of the drop ($\xi = \xi_0$), where the solution for the first-order temperature correction outside the drop can be written as (see Appendix C)

$$T_{1\,\mathrm{air}} = \sum_n \Lambda^{(a)}_n \Xi^a_n[\xi]\, P_n[u]. \tag{62}$$

In such a way we obtain the system of equations

$$\begin{aligned} \Lambda^{(a)}_n \Xi^{(a)}_n\big|_{\xi=\xi_0} &= \Big\{ \sum_k W^{(1)}_{n,k} \Xi^{(1)}_k + \Lambda^{(1)}_n \Xi^{(1)}_n \Big\}_{\xi=\xi_0}, \\ \kappa \Lambda^{(a)}_n \partial_\xi \Xi^{(a)}_n\big|_{\xi=\xi_0} &= \Big\{ \sum_k W^{(1)}_{n,k} \partial_\xi \Xi^{(1)}_k + \Lambda^{(1)}_n \partial_\xi \Xi^{(1)}_n \Big\}_{\xi=\xi_0}, \end{aligned} \tag{63}$$

from which we find

$$\Lambda^{(1)}_n = \left\{ \frac{\kappa \frac{\sum_k W^{(1)}_{n,k} \Xi^{(1)}_k}{\Xi^{(a)}_n} - \frac{\sum_k W^{(1)}_{n,k} \partial_\xi \Xi^{(1)}_k}{\partial_\xi \Xi^{(a)}_n}}{\frac{\partial_\xi \Xi^{(1)}_n}{\partial_\xi \Xi^{(a)}_n} - \kappa \frac{\Xi^{(1)}_n}{\Xi^{(a)}_n}} \right\}_{\xi=\xi_0}. \tag{64}$$

Thus, we derived the distribution of the temperature deviations T_1 inside the drop. This allows us to find the general stationary solution for the stream functions, and to analyze its stability relative to the increase of the initial temperature gradient.

C. General stationary solution

Now, having in hand the analytical expressions for the temperature distribution within the ellipsoidal drops, we can solve explicitly the Marangoni boundary conditions (32) and (33). After substitution of the components v_u, v_ξ from Eqs. (35) and (45) to Eqs. (32) and taking into account that at the drop boundary $v_\xi = 0$ ($\xi = \xi_0$), we obtain the general expression for Marangoni boundary condition at the free surface of the drop

$$-\frac{h_u}{h_\xi}\partial_\xi \frac{\partial_\xi \psi}{h_\xi h_\varphi h_u} = -\mathrm{Ma}\, \frac{\partial_u T}{h_u} \quad (\text{at } u \in [u_0, 1]). \tag{65}$$

In view of Eq. (65) the system of Eqs. (32) and (33) can be rewritten in the form

$$\left\{ 2\xi\, \partial_\xi \psi - (u^2+\xi^2)\partial^2_\xi \psi = -\mathrm{Ma} \frac{(u^2+\xi^2)^{3/2}}{\sqrt{1+\xi^2}} (1-u^2)\partial_u T \right\}_{\xi=\xi_0} \quad (\text{at } u \in [u_0, 1]), \tag{66}$$

$$\partial_\xi \psi = 0 \quad (\text{at } \xi = \xi_0,\ u \in [-1, u_0]), \tag{67}$$

where Ma is the Marangoni number, defined earlier in Eq. (19). Estimating the contributions to the right part of Eq. (66) and taking into account the solutions for (ψ, T_0, T_1), we obtain that for the typical parameters of the system $\mathrm{Ma} \ll 10^3$. In this case the contribution from the temperature deviation T_1 in solving of the Marangoni boundary condition is negligibly small comparatively to that from T_0 and can be omitted. This confirms the validity of the condition (24) corresponding to Boussinesq approximation. The same is true for the inequality (23) with account to the typical parameters of the system [72]. Hence, the full stationary solution for the stream function in the main approximation can be written either as expansion over initial basic functions ψ_i,

$$\psi = \sum_{i=3}^{N_r} c_i\, \psi_i, \tag{68}$$

or over the basic functions $\psi_{i,st}$, satisfying to the condition of sticking at the bottom surface,

$$\psi = \sum_{i=3}^{N_r} c_{i,st}\, \psi_{i,st}, \tag{69}$$

where N_r is the number of basic functions used in the summation. Now we have two ways to find the stream function ψ.

The first one is straight: to substitute expansion (68) in the system (66) and (67) and to find the set of c_i, satisfying the following system of equations:

$$\begin{aligned} &\left(\partial_\xi - \frac{1}{2\xi_0}\left(\xi_0^2 + u^2\right) \partial^2_\xi \right) \psi \Big|_{\xi=\xi_0} \\ &\quad = \underline{\sum_j \hat{O}^{\mathrm{free}}_{ij} \mathcal{F}_i[u] c_j} = -\mathrm{Ma}\, \frac{\left(\xi_0^2+u^2\right)^{3/2}}{2\xi_0\sqrt{1+\xi_0^2}}\, \frac{(1-u^2)}{2} \\ &\quad = \underline{r[u]}, \quad (\text{at } u \in [u_0, 1]), \end{aligned} \tag{70}$$

$$\sum_{i,j} \hat{O}^{\mathrm{stick}}_{ij} c_j \mathcal{F}_i[u] = 0 \ \ (\text{at } u \in [-1, u_0]), \tag{71}$$

where we introduced an expansion of the left part of the Marangoni condition (70) over the set of functions $\mathcal{F}_i[u]$ using the matrix representation $\hat{O}^{\mathrm{free}}_{ij}$ at the free boundary of a drop for $\xi = \xi_0$. To obtain the right part of Eq. (70) we substituted expression (56) for the temperature distribution T_0 to the right part of the first equation in the system (66). The matrix $\hat{O}^{\mathrm{free}}_{ij}$ describes the action of the operator $[\partial_\xi - \frac{1}{2\xi_0}(\xi_0^2 + u^2)\,\partial^2_\xi]$ on the expansion (68) for the stream function ψ at $\xi = \xi_0$. In turn, the matrix $\hat{O}^{\mathrm{stick}}_{ij}$ describes the action of the operator ∂_ξ on the expansion (68) for the stream function ψ at $\xi = \xi_0$. In

Eq. (70) we introduced two new definitions (underlined as ...), which are used to simplify the further derivations.

We note that the irrationality $(\xi_0^2+u^2)^{3/2}$ is present in the right part of Eq. (70), i.e., in the $r[u]$, but this irrationality is absent in the functions $\{\mathcal{F}_i[u]\}$ [see expression (43)], determining the dependence of the left part of this equality on u. This means that the full solution of the system (70) is the infinite series. However, we able to obtain only the finite approximation for this solution. The series is breaking once the following convergence criterion is satisfied: the sum of the norms $E[\{c_j\}]^{\text{free}}$, $E[\{c_j\}]^{\text{stick}}$ of deviations of Eqs. (71) from zero,

$$
\begin{aligned}
E[\{c_j\}]^{\text{free}} &= \int_{\text{free}} \frac{du}{1-u^2}\left(\hat{O}_{ij}^{\text{free}} c_j \mathcal{F}_i[u] - r[u]\right)^2 \\
&= \hat{O}_{ij}^{\text{free}} \hat{O}_{km}^{\text{free}} c_j c_m \underbrace{\int_{\text{free}} \frac{du}{1-u^2} \mathcal{F}_i \mathcal{F}_k}_{F_{ik}^{\text{free}}} \\
&\quad - 2\hat{O}_{ij}^{\text{free}} c_j \underbrace{\int_{\text{free}} \frac{du}{1-u^2} r[u]\mathcal{F}_i[u]}_{R_i} \\
&\quad + \int_{\text{free}} \frac{(r[u])^2}{1-u^2}\, du, \\
E[\{c_j\}]^{\text{stick}} &= \int_{\text{stick}} \left(\hat{O}_{ij}^{\text{stick}} c_j \mathcal{F}_i[u]\right)^2 \frac{du}{1-u^2} \\
&= \hat{O}_{ij}^{\text{stick}} \hat{O}_{km}^{\text{stick}} c_j c_m \hat{F}_{ik}^{\text{stick}},
\end{aligned}
\tag{72}
$$

should be minimal for the obtained N_r-measured set of c_i,

$$
\begin{aligned}
\partial_{c_\alpha} E[\{c_j\}] &= 2\underbrace{\hat{O}_{k\alpha}^{\text{free}} \hat{F}_{ki}^{\text{free}} \hat{O}_{ij}^{\text{free}}}_{M_{\alpha j}^{\text{free}}} c_j - 2\underbrace{\hat{O}_{i\alpha}^{\text{free}} R_i}_{V_\alpha} \\
&\quad + 2\underbrace{\hat{O}_{k\alpha}^{\text{stick}} \hat{F}_{ki}^{\text{stick}} \hat{O}_{ij}^{\text{stick}}}_{M_{\alpha j}^{\text{stick}}} c_j \\
&= 0 \;\rightarrow\; (\hat{M}^{\text{stick}} + \hat{M}^{\text{free}})|c\rangle = |V\rangle,
\end{aligned}
\tag{73}
$$

where $|c\rangle$ and $|V\rangle$ are designations of the corresponding columns. The above expressions can be essentially simplified with account to expression (D5).

Applying the above procedure the main approximation for the stream functions with the given accuracy of determination are obtained (relative deviations of norms $E[\{c_j\}]^{\text{free}}$, $E[\{c_j\}]^{\text{stick}}$ from zero are about 10^{-3}; see Figs. 13–15). The deviations $E[\{c_j\}]^{\text{free}}$ and $E[\{c_j\}]^{\text{stick}}$ converge to zero when the number of the basis functions N_r increases ($N_r \to \infty$; see Fig. 13). This fact confirms the regular convergence provided by our procedure and correctness of our approach in derivation of the general solution for the stream function.

Additionally, an improved representation of the velocities and temperature distribution corresponding to the stationary thermocapillary convection within the ellipsoidal drop in dependence on the values of ξ_0, κ and u_0 are calculated (Figs. 16–19). It is instructive to analyze the differences in the velocity distribution within Marangoni vortices between the geometries with $u_0 = 0$ and $u_0 \neq 0$, for which the drop surface with the sticking boundary condition partly overlaps the circular edge of a drop. This is a realistic scenario due to

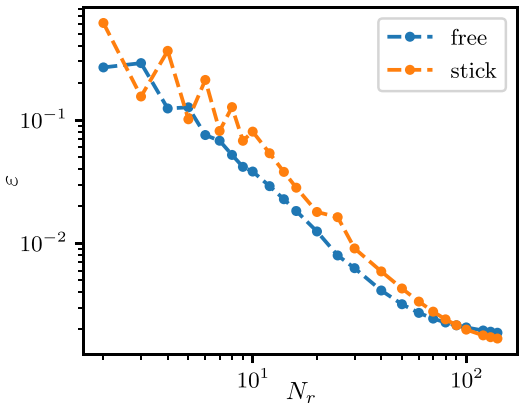

FIG. 13. Illustration of the convergence of the expansion procedure for the stream function in dependence on the number of the basic functions. Dependence of the relative error ε in deviations of norms $E[\{c_j\}]^{\text{free}}$, $E[\{c_j\}]^{\text{stick}}$ from zero (Ma $= 1$, $\xi_0 = 0.1$).

the presence of a bulky smectic meniscus connecting the drop with smectic film (Figs. 1 and 4). Moreover, this is important for understanding of the influence of the shape of the end face of the drop on the thermocapillary convection within it. In Figs. 16 and 17 the convection patterns correspond to the case when the no-slip boundary conditions extend along the drop surface towards its upper part ($u_0 = 0.25$). Contrary to this, in Figs. 18 and 19 the sticking boundary conditions at the bottom drop surface terminate exactly at the circular edge of the drop. It is readily seen that in the first case the convection vortices are not able to penetrate in the end face of the ellipsoidal drop (see Figs. 16 and 17). This indicates that the shape of the butt end of the drop is not important for such a case. The differences in the stream function patterns between the geometries with $u_0 = 0$ and $u_0 \neq 0$ are highlighted in Fig. 20. One can see that these differences show up themselves only in a butt end region of the drop, and do not affect the convection motion in the main volume of the drop.

The second way to obtain the full stream function is to use the set of functions $\psi_{i,st}$ [see Eq. (69)]. It is possible for $u_0 = 0$. It is clear that the functions $\psi_{i,st}$ automatically satisfy the sticking boundary condition ($\partial_\xi \psi = 0$) at the bottom drop

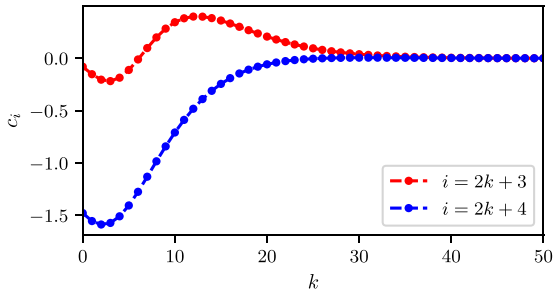

FIG. 14. Coefficients in decomposition of the stream function ψ for even and odd basic solutions (Ma $= 1$, $\xi_0 = 0.1$, $u_0 = 0.1$). Illustration of the convergence of the expansion of the solution for ψ over basic functions in dependence on their number i as a function of a current integer number k. Both even and odd basic solutions are shown; the convergence is reached for k values about 25.

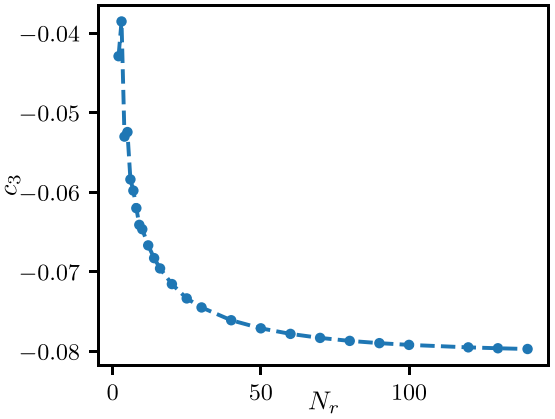

FIG. 15. Convergence of the coefficient c_3 of the expansion of the final stream function over the basic functions in dependence on their number(Ma = 1, $\xi_0 = 0.1$).

surface, the second equation in a system of Eqs. (67). Therefore, the only thing we need is to resolve the first equation in a system (67). The Marangoni boundary condition at the top (free) surface reads

$$\left[\partial_\xi - \frac{1}{2\xi_0}\left(\xi_0^2 + u^2\right)\partial_\xi^2\right]\psi\Big|_{\xi=\xi_0} = \underline{\sum_{i,j} \hat{O}_{ij}^{\text{free}} \mathcal{F}_i c_{j,st}} = -\text{Ma}\,\frac{\left(\xi_0^2 + u^2\right)^{3/2}}{2\xi_0\sqrt{1+\xi_0^2}}\,\frac{(1-u^2)}{2} = \underline{r[u]}. \tag{74}$$

Similarly to that was done earlier, we substituted expression (56) for the temperature distribution T_0 to the right part of the first equation in the system (67). Again, we need to find the constants $c_{i,st}$ of the expansion of the full stream function over basic functions $\psi_{i,st}$. By analogy with the previous case we find the finite approximation for this solution. The series is broken once the following convergence criterion is satisfied: the norm of deviation of the Eq. (74) from zero,

$$E[\{c_{j,st}\}] = \int \left[\sum_{i,j} \hat{O}_{ij}^{\text{free}} \mathcal{F}_i c_{j,st} - r(u)\right]^2 \frac{du}{1-u^2}, \tag{75}$$

should be minimal for the N_r-measured set of $c_{i,st}$, (details of calculation of $E[\{c_{j,st}\}]$ are presented in Appendix F). The

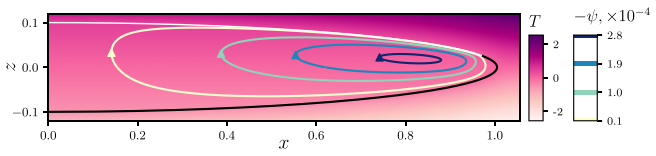

FIG. 16. Streamlines and temperature distribution for the generalized thermocapillary convection within the drop ($\xi_0 = 0.1$, $\kappa = 0.2$, $u_0 = 0.25$, Ma = 1, $N_r = 110$; $\kappa = \varkappa_{\text{air}}/\varkappa$ is a relative heat conductivity); the color scale for the temperature is characterized by a more saturated light-purple in a hot areas). The sticking boundary conditions are extended above the circular edge of a drop (bold black line).

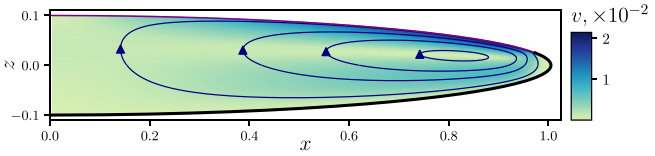

FIG. 17. Modulus of velocity for the generalized thermoconvection flow within the drop ($\xi_0 = 0.1$, $u_0 = 0.25$, $\kappa = 0.2$, Ma = 1, $N_r = 110$). The dimensional values of v can be deduced using the corresponding scaling parameter $\chi/H = 4 \times 10^{-3}$ m s^{-1}. The circulation period Δt for certain velocities can be determined from the integral over the closed trajectory of the motion as shown in the Discussion. In dimensionless form Δt values are 124, 151, 206, and 484 as counted off from the center of the vortex to its periphery, respectively (from dark streamline to light one in Fig. 16). The dimensional values of Δt can be obtained using the corresponding scaling parameter $\Delta t = ((H^2/2)(\xi_0\,\chi)^{-1})\,\Delta\widetilde{t}$, $(H^2/2)(\xi_0\,\chi)^{-1}$, which is about 0.0125 s for the typical geometrical and material characteristics of the drop. In seconds they constitute 1.55 s, 1.89 s, 2.575 s, and 6.05 s, respectively.

above deviation $E[\{c_{j,st}\}]$ converges to zero when the number of the basic functions $N_r \to \infty$. The results obtained for the stream functions and velocity distributions within the drop by a second method of calculations are closely the same as shown in Figs. 16–19.

D. Stability of the stationary solution. Crossover to the limit of the plane fluid layer

After the stationary solutions for the thermocapillary flows within isotropic fluid droplets in FSSFs are determined ($\psi = \psi_1 + \cdots$, $T = T_0 + T_1 + \cdots$), the natural question about stability of these solutions relative to the increase of the initial temperature gradient (i.e., increasing of the Marangoni number, Ma) arises. To answer this question let us imagine that the hydrodynamic characteristics of the system in certain moment slightly deviate from those of the stationary solution. Our aim is to trace the evolution of these deviations with time.

The partial solutions of the Eqs. (15)–(18) can be written in the form of normal pertubations which have exponential dependence on time [2,8,45,70,73],

$$v_\mu \propto \exp[\lambda t], \tag{76}$$

$$T_1 \propto \exp[\lambda t], \tag{77}$$

where exponent λ determines the time character of perturbation evolution. The normal perturbations with the negative sign of the real part of λ are decaying, while the perturbations with the positive sign of the real part of λ correspond to

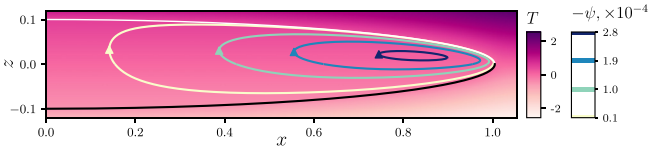

FIG. 18. Streamlines and temperature distribution (color map) for the generalized movement of thermocapillary convection ($\xi_0 = 0.1$, $u_0 = 0$, $\kappa = 0.2$, Ma = 1, $N_r = 110$).

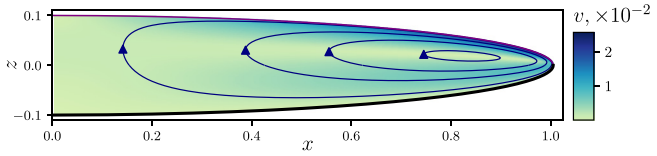

FIG. 19. Modulus of velocity for the generalized thermoconvection flow within the drop ($\xi_0 = 0.1$, $u_0 = 0$, Ma $= 1$, $N_r = 110$). The circulation period Δt for certain velocities in dimensionless form is 135, 156, 206, and 489 as counted off from the center of the vortex to its periphery (from dark streamline to light one in Fig. 18). The dimensional values of Δt constitute 1.69 s, 1.95 s, 2.58 s, and 6.11 s, respectively.

the growing fluid motions. Then, the stationary solutions for the thermocapillary motion are stable if the condition for all solutions $\mathrm{Re}[\lambda] < 0$ is fulfilled. However, the spectrum of perturbations depends on the value of the Marangoni number, Ma. While for a small Ma values all λ_i possess the negative sign of the real part of lambda, starting from the some larger Ma the perturbations with the positive $\mathrm{Re}[\lambda]$ arrive. Thus, the margin of stability of thermocapillary flow is determined by a minimal Marangoni number Ma_c for which the normal perturbation (ψ_c, T_c) reaches the zero $\mathrm{Re}[\lambda]$ value for a first time. To find the stability limit we introduce the general expansions $(\psi_\Sigma = \psi + \psi_c, T_\Sigma = T + T_c)$ and substitute them in Eqs. (15)–(18) in order to make a linearization procedure over (ψ_c, T_c). We note that the equation $\hat{E}^4\psi_c = 0$ over ψ is linear initially, thus, the basis of the solution for ψ_c remains the same. This means that we use the same expansion $\psi_c = \sum_j c_{cj}\psi_{j,st}$ over $\{\psi_{j,st}\}$, which is a set of basic functions, corresponding to the sticking conditions at the bottom surface of a fluid drop (see Sec. IV A and Appendix F).

The equation $\Delta T_\Sigma = \frac{c}{H}(\mathbf{v_\Sigma}\nabla)T_\Sigma$ for the critical temperature distribution after linearization takes the form

$$\Delta T_c = \frac{c}{H}(\mathbf{v}_c\nabla)T_0, \tag{78}$$

where the terms $\frac{c}{H}(\mathbf{v}_c\nabla)T_1$ and $\frac{c}{H}(\mathbf{v}_1\nabla)T_c$ are omitted due to a higher order of smallness. Thus, for the case $\mathrm{Ma} \ll 10^3$, Eq. (78) is coincides with Eq. (50) which allows the temperature amendments of the first order to be calculated as a response to a set $\{c_{cj}\psi_{j,st}\}$; in such a way we obtain an expansion $T_c = \sum_j c_{cj}T_{1\,j}$.

At the next step it is necessary to find the critical Ma_c and corresponding vector $\{c_{cj}\}$, in order to satisfy Marangoni

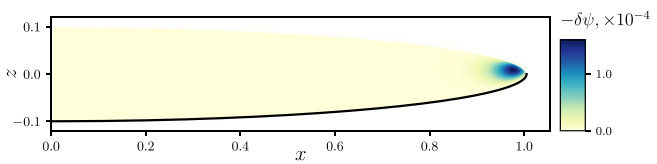

FIG. 20. Difference of streamlines ψ for the generalized thermoconvection flow within the drop for $u_0 = 0$ and $u_0 = 0.25$, ($\xi_0 = 0.1$, $\kappa = 0.2$, Ma $= 1$, $N_r = 110$).

boundary condition (65) at $\xi = \xi_0$:

$$\left\{\partial_\xi\psi_c - \frac{1}{2\xi}(\xi^2+u^2)\,\partial_\xi^2\psi_c\right\}_{\xi=\xi_0} = -\mathrm{Ma}_c\left\{\frac{(u^2+\xi^2)^{3/2}}{2\,\xi\,\sqrt{1+\xi^2}}(1-u^2)\,\partial_u T_c\right\}_{\xi=\xi_0}, \tag{79}$$

where in accordance with expression (61) and with account to equality (D6) each $\partial_u T_{1j}$ can be written as

$$\partial_u T_{1j} = -\sum_n\left[\sum_k \left(W^{(1)}_{n,k}\right)_{j,st}\Xi^{(1)}_k + \left(\Lambda^{(1)}_n\right)_{j,st}\Xi^{(1)}_n\right] \times \frac{n(n+1)}{1-u^2}\mathcal{F}_n[u]. \tag{80}$$

For simplification we designate the right part of the equality (79) as $\mathrm{Ma}_c\sum_j r_j[u]\,c_{cj}$. In such a way Eq. (79) can be rewritten as

$$\left(\partial_\xi - \frac{1}{2\xi_0}(\xi_0^2+u^2)\partial_\xi^2\right)\psi_c\Big|_{\xi=\xi_0} = \sum_{i,j}\hat{O}^{\mathrm{free}}_{ij}\mathcal{F}_i\,c_{cj} = \mathrm{Ma}_c\sum_j r_j[u]\,c_{cj}. \tag{81}$$

Similarly to the previous section, we are searching for the solutions for which the norm of deviation from Eq. (81) turns to zero:

$$\mathcal{L} = \sum_{jm} c_{cj}c_{cm}\Bigg\{\underbrace{\sum_{i,l}\int \hat{O}^{\mathrm{free}}_{ij}\mathcal{F}_i\hat{O}^{\mathrm{free}}_{lm}\mathcal{F}_l\,\frac{du}{1-u^2}}_{\hat{M}^{(0)}_{jm}} - \mathrm{Ma}_c\underbrace{\int\left[\sum_i \hat{O}^{\mathrm{free}}_{ij}\mathcal{F}_i\,r_m[u] + \sum_l \hat{O}^{\mathrm{free}}_{lj}\mathcal{F}_l r_j[u]\right]\frac{du}{1-u^2}}_{\hat{M}^{(1)}_{jm}} + \mathrm{Ma}_c^2\underbrace{\int r_j[u]r_m[u]\frac{du}{1-u^2}}_{\hat{M}^{(2)}_{jm}}\Bigg\} = 0. \tag{82}$$

The vector $\{c_{cj}\}$ and the corresponding minimal critical value Ma_c can be determined from Eq. (82) for $\mathcal{L}$. This equation can be rewritten in the form

$$\left(\hat{M}^{(0)} - \mathrm{Ma}_c\,\hat{M}^{(1)} + \mathrm{Ma}_c^2\,\hat{M}^{(2)}\right)|c_c\rangle = 0, \tag{83}$$

where the components of matrices $\hat{M}^{(0)}, \hat{M}^{(1)}, \hat{M}^{(2)}$ are determined in expression (82) as the interlinear (footnote) designations. Thus, our problem is reduced to the quadratic eigenvalue problem [74]. The standard method of its solution is a reduction to the generalized eigenvalue problem (see Appendix F). However, there is a certain complication in its solution: the obtained Ma, are complex numbers, containing real and imaginary parts, due to the irrationality in the left part of Eq. (79). To overcome the above problem we used one of the properties of our system, lying in the fact that an increase of the number of the basic functions N_r leads to the diminishing of the image part of Ma_c; it turns to zero when $N_r \to \infty$. In practice, we search for the solution depending

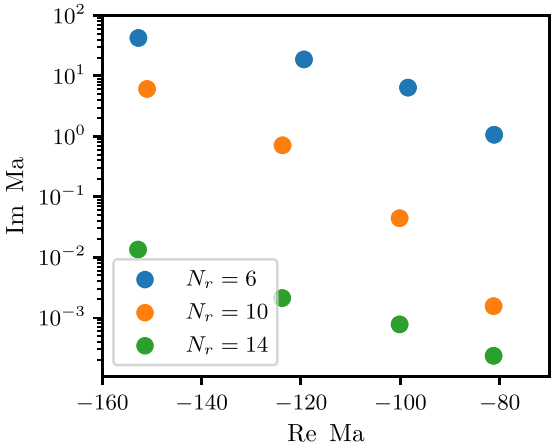

FIG. 21. Illustration that the image part of the Marangoni number, Ma, decreases with the increase of the number N_r of the accounted basic functions (four lowest values of Ma spectrum for each N_r are presented, $\xi_0 = 0.1$, $\kappa = 0.2$).

on the number N_r of the basic functions, for which the image part of Ma would be less than 10^{-3}. The illustration of the progress in these calculations is shown in Fig. 21. The negative value of the critical Marangoni number Ma_c is not accidental. This means that for the case under consideration the temperature of the free drop surface is higher than that at the bottom surface with the sticking (no-slip) conditions, the stationary thermocapillary convection is stable.

As was mentioned in Introduction, the vast amount of papers devoted to Marangoni convection is focused on a rather simple case of a flat fluid films. Our previous paper on thermocapillary convection within isotropic droplets in FSSFs exploited the same approximation. The formalism of the stream functions which we successfully applied to study the Marangoni convection in ellipsoidal drops provides a unique possibility to investigate a crossover from the lenslike drop to a flat fluid layer. This is made by reducing of the droplet ellipticity ratio ξ_0 that leads in the limit $\xi_0 \to 0$ to the case of a flat fluid film. The phase diagram for Ma_c as a function of the ellipticity parameter ξ_0 for different values of the relative heat conductivity κ is shown in Fig. 22. The modulus of the obtained value $\mathrm{Ma}_c \approx -50$ for $\kappa \to 0$ matches well with the case $\mathrm{Ma}_c \sim 50$ described in the literature for

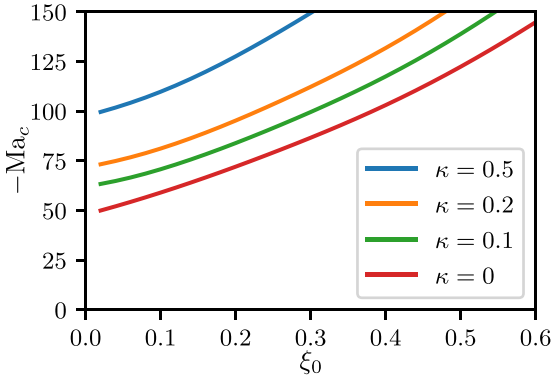

FIG. 22. Phase diagram for the critical Marangoni number Ma_c as a function of the ellipticity ratio ξ_0 for different values of the relative heat conductivity κ .

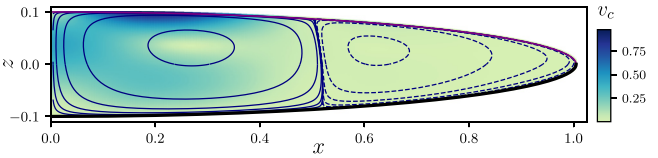

FIG. 23. Critical Marangoni flows in the ellipsoidal drop ($\xi_0 = 0.1$, $\kappa = 0.2$, $\mathrm{Ma}_c = -81.2$). The dashed and solid lines indicate the opposite direction of the fluid velocity in the neighboring vortices.

a flat fluid film placed on a heat-insulating hard substrate with the sticking conditions [8]. The results of calculations of streamlines and velocities for the negative Ma_c values are presented in Figs. 23–25. According to our calculations with diminishing of the ellipticity ratio ξ_0 the amount of vortices in the direction of the axial drop cross section progressively increases (see Figs. 23–25). The number of basic functions, which is necessary for an accurate convergence of the calculation procedure, is estimated as $N_r \sim \xi_0^{-1}$. These calculations are in good agreement with the results of our previous paper [47], where the formation of about six convection cells (rolls) along the lateral drop size was predicted.

E. Numerical experiment

To get further insight about Marangoni flows within ellipsoidal isotropic droplets embedded in FSSFs we carried out the numerical calculations, which took the real shape of the drops and their material and transport properties into account. The details of the numerical experiment are presented in Appendix G. In short, to simulate the thermocapillary flow within the drops we used the cylindrical coordinates (r, ϕ, z). In the problem under consideration, the transfer of mass and heat does not depend on the angular coordinate ϕ. This allows us to consider the hydrodynamic problem as a two-dimensional and proceed with the numerical calculations in the coordinates (r, z). In such formulation, the geometry of the lenslike droplet is described by an ellipse with a semimajor axis $a = R_b$, and a semiminor axis $b = 0.5H$ (see Table I).

The hydrodynamic flows in the droplet are described as follows. The Navier-Stokes and the continuity equations for the incompressible fluid, as well as the heat transfer equation are written in the cylindrical coordinates. The stream function ψ in this case satisfies the relations $\partial\psi/\partial z = ru$ and $\partial\psi/\partial r = -rv$, where u and v are the horizontal and the vertical components of the liquid flow velocity, respectively. The vorticity is introduced in cylindrical coordinates as $\omega = \partial u/\partial z - \partial v/\partial r$. At the end, the mathematical model consists of three equations, which are solved with respect to three

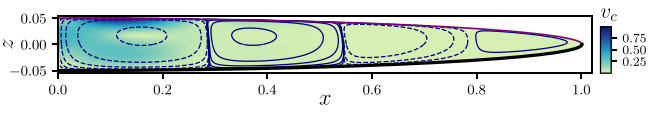

FIG. 24. Critical Marangoni flows in the ellipsoidal drop ($\xi_0 = 0.05$, $\kappa = 0.2$, $\mathrm{Ma}_c = -75.9$). The dashed and solid lines indicate the opposite direction of the fluid velocity in the neighboring vortices.

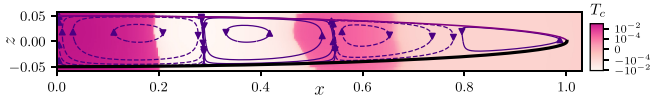

FIG. 25. Streamlines and temperature distribution (the logarithmic color scale for the temperature is characterized by more saturated light purple in hot areas) for the critical Marangoni flows in the ellipsoidal drop ($\xi_0 = 0.05, \kappa = 0.2, \mathrm{Ma}_c = -75.9$). The dashed and solid lines indicate the opposite direction of the fluid velocity in the neighboring vortices.

variables: ω, ψ and temperature T. The above equations are accompanied by a set of initial and boundary conditions, also written in cylindrical coordinates.

To solve numerically the Marangoni convection problem the commercial package FlexPDE Professional Version 7.18/W64 3D was used [75]. The mathematical algorithm is based on the Galerkin finite element method with application of the modified iterative Newton-Raphson method [76]. The time intervals in the program are generated automatically in order to minimize the calculation error. To secure the solution reliability the special attention to the mesh convergence was paid (see Appendix G).

The calculations were performed for the time $t_{\max} = 20\, t_{\mathrm{rel}}$, $\mathrm{Ma} = 1$ and correspond to the stationary regime (t_{rel} is the heat relaxation time in the air due to the thermal conductivity; see Appendix G). This time is enough for the system to reach the stationary state. The later is achieved due to a fact that the thermal conductivity dominates over the convective heat transfer for the considered values of the material and geometric parameters, of the drops and their environment. According to numerical calculations, the maximum velocity of the convective transfer is $v_{\max} \approx 10^{-5}$ m/s. Then the convective transfer time can be evaluated as $t_{\mathrm{conv}} = R_b/v_{\max} \approx 10$ s. To estimate the heat transfer time determined by thermal conductivity we use the value of the fluid thermal conductivity $\chi \approx 4 \times 10^{-8}$ m^2/s to obtain the corresponding time $t_{\mathrm{cond}} = R_b H/\chi \approx 0.05$ s. It is readily seen that $t_{\mathrm{cond}} \ll t_{\mathrm{conv}}$, thus confirming our initial claim of predominance of the thermal conductivity. The results of the numerical calculations presented below are obtained for the time $t = t_{\max}$.

In our numerical calculations we considered the case for which the smectic shell (substrate) is in contact with the lower surface of isotropic droplet, while the upper interface is free (Figs. 1 and 4). This situation is realized for $T_{up} > T_{dn}$ (see Sec. II B), so the values $T_{up} = 334$ K and $T_{dn} = 324$ K were chosen for further calculations. By default, the Marangoni boundary condition (Appendix G) was used for the free (upper) surface of the droplet. Contrary to this, the boundary no-slip (sticking) condition (Appendix G) was used for the case the smectic shell (substrate) was in immediate contact with the lower surface of a drop and for the cut end of the fluid lens. The corresponding temperature distribution is shown in Fig. 26. In accordance with our calculations the shape of the droplet does not show any significant effect on the temperature distribution in the droplet for the values of the parameters used. In Fig. 27 the distribution of the fluid flow velocity in droplets is shown for different types of droplet shapes.

According to Fig. 26, the temperature decreases along the upper (hot) surface of the droplet and conversely increases at its lower (cold) surface when going in the direction from the symmetry axis to the edge of the droplet along the radial coordinate r. Again, there are no noticeable quantitative differences in the temperature distribution along the radius r for the different shapes of the droplet.

The fluid flow circulating in the (r, z) plane is directed clockwise in the case under consideration (Fig. 27). Because $T_{up} > T_{dn}$, the Marangoni flow is directed along the free surface of the droplet from the hot area to the cold area, (i.e., from the area of the low surface tension to the area of the high surface tension). It is important that the no-slip (sticking) condition at the boundary between the smectic and the isotropic liquid slows down the thermocapillary flow.

The corresponding stream functions are presented in Fig. 28 for several consecutive time points. There are no qualitative differences in the plots of the stream function ψ between different time periods. We observe one axially symmetric vortex in the ellipsoidal drop that is in agreement with our analytical results (Figs. 16–19). The quantitative differences are due to a fact that the flow velocity gradually

TABLE I. Problem parameters.

Symbol	Parameter	Value [unit of measurement]
$\varkappa$	Thermal conductivity of liquid	0.12 [W/(mK)]
$\varkappa_a$	Thermal conductivity of air	0.026 [W/(mK)]
c_p	Specific heat capacity of liquid	2500 [J/(kg K)]
c_a	Specific heat capacity of air	1000 [J/(kg K)]
η	Dynamic viscosity	1.4×10^{-2} [s Pa]
ρ	Liquid density	1200 [kg/m^3]
ρ_a	Air density	1.2 [kg/m^3]
ς	Tension temperature coefficient	1.0×10^{-4} [N/(m K)]
H	Droplet height	20 [μm]
H_{out}	Domain height	1 [mm]
R_b	Droplet radius	100 [μm]
R_{out}	Domain radius	1 [mm]
T_{dn}	Bottom plate temperature	324 [K]
T_{up}	Top plate temperature	334 [K]

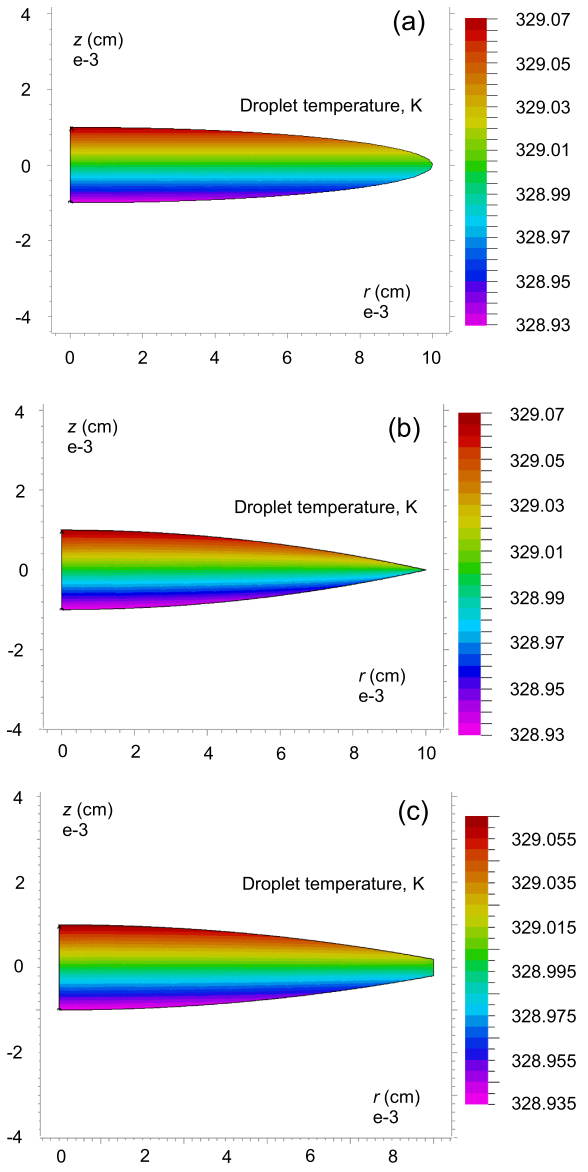

FIG. 26. Temperature distribution within the isotropic droplets; the smectic shell is in contact with the bottom surface of isotropic droplet (a, b, c). The droplet shapes: ellipse (a), a biconvex lens (b), and a lens with the cut end at the edge (c).

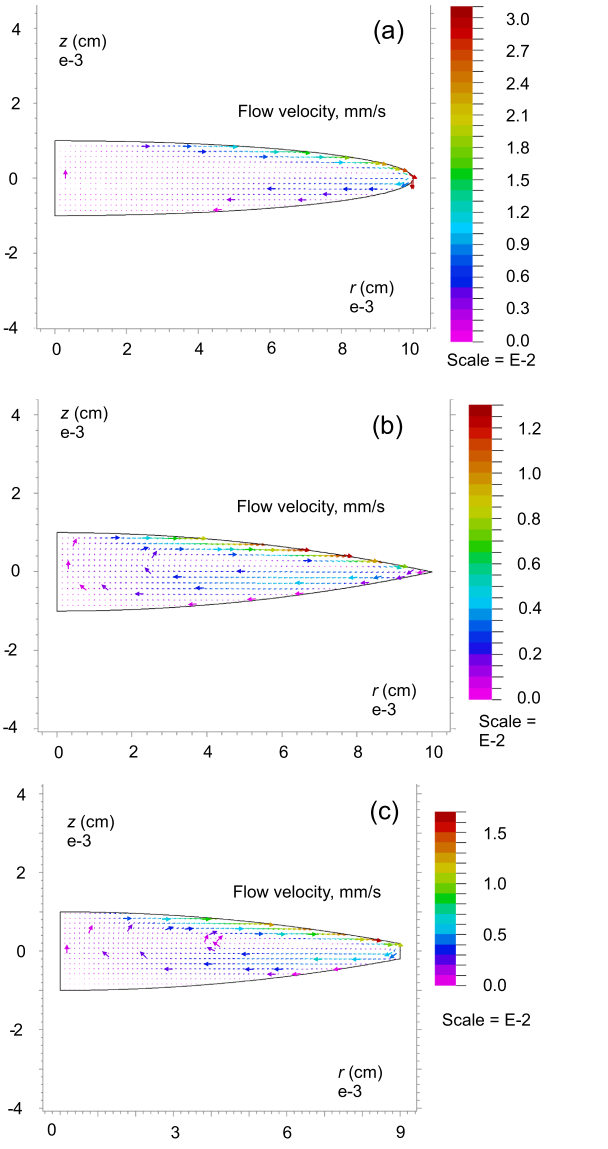

FIG. 27. Distribution of the fluid flow velocity within the isotropic droplets; the smectic shell is in contact with the bottom free surface of isotropic droplet (a, b, c). The droplet shapes: ellipse (a), biconvex lens (b), and a lens with the cut end at the edge (c).

increases until it reaches a stationary state. We conclude that numerical results for Marangoni convection within ellipsoidal droplets in FSSFs are in good accordance with that obtained by analytical methods in Sec. IV.

V. DISCUSSION

We have developed a hydrodynamic theory of the Marangoni flow in the axially symmetric ellipsoidal fluid droplets on the basis of the formalism of the Stokes stream functions. This approach was applied to ellipsoidal isotropic drops spontaneously formed in overheated FSSFs and to droplets of insoluble fluids (of the type of oil or glycerol) deposited on it. The asymmetric geometry for which the upper drop interface is connected with the air, while its bottom surface is in contact with the static smectic layering is considered. This situation can be implemented experimentally when the temperature of the upper side of the film is higher than the lower one. Due to the nonuniform temperature distribution the tangential Marangoni force always exists at the free drop surface. This leads to a fluid flow along its curved interface which is possible for the arbitrarily small Marangoni numbers. The thermocapillary flow occurs along the free surface of the droplet from the hot area to the cold one, leading to the formation of the individual torroidal-like vortices within the drop. Our calculations indicate that the no-slip (sticking) condition at the boundary between the smectic and isotropic fluid slows down the circulatory Marangoni flow.

There is another item related to the implementation of no-slip (sticking) boundary conditions at the interface between the fluid and smectic substrate. In Sec. II B we have shown

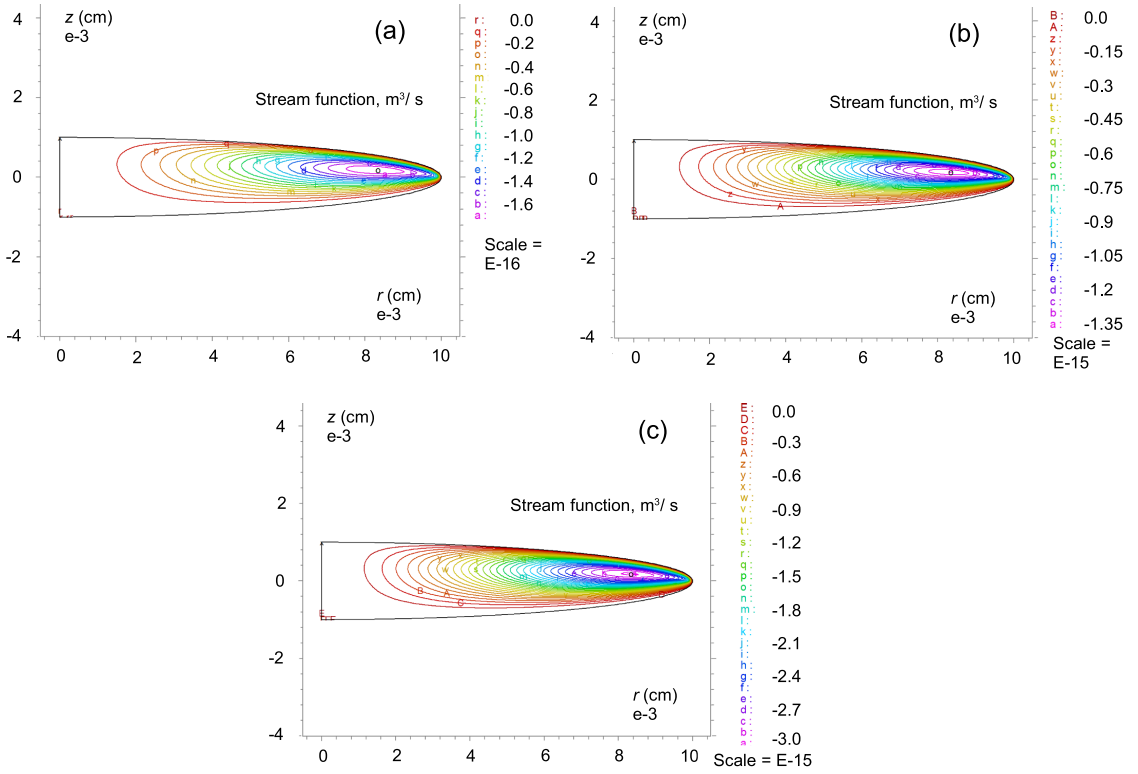

FIG. 28. Stream functions for the ellipsoidal drop with a smectic film on the bottom free surface: (a) $t = 0.1t_{\rm rel}$, (b) $t = 0.5t_{\rm rel}$, and (c) $t = 20t_{\rm rel}$.

that for the model of a fluid drop and its environment used in our theoretical analysis the tangential component of the smectic elastic force compensates the Marangoni force at the fluid-smectic interface. This effectively hinders the flow of the smectic material and leads to sticking of fluid motion at the border with a smectic shell. In principle, there is another possibility for the smectic motion, so called, permeation, i.e., the flow of the material through the smectic layers [45,57], which is usually disregarded due to its low velocity. Our estimations actually indicate the case; in the limit of small value of the permeation constant $\lambda_p \simeq 10^{-16}$ m^2 Pa^{-1} s^{-1} the permeation velocity can be written as $v_{\rm perm} \sim {\rm D}_T\, A\, T^{-1}$ [45,57], where $\rm D_T$ and A are the thermodiffusion coefficient and the temperature gradient across the drop, respectively. Using the typical values ${\rm D}_T \sim 10^{-10}$ m^{2}s^{-1}, $A = 10^4$ K m^{-1}, and $T = 300$ K we obtain $v_{\rm perm} \sim 10^{-9}$ m s^{-1}. According to our calculations, the maximum velocity of the convection flow is $v_{\rm max} \sim 10^{-5}$–10^{-4} m s^{-1}. Thus, $v_{\rm perm} \ll v_{\rm max}$, confirming our initial assertion that permeation process in smectics is too slow. We conclude that permeation in smectics cannot provide the Marangoni transport at the fluid-smectic interface confirming our assumption of the sticking conditions at this interface.

One of the lines of our research is to study the stability of the stationary solutions for the thermocapillary convection within ellipsoidal fluid droplets (Sec. IV D). According to our results, the obtained stationary solutions for the fluid drop with the sticking boundary conditions at the bottom interface and $T_{dn} < T_{up}$ are stable. This result remains valid upon a crossover from the ellipsoidal droplets to a flat fluid layer. Such a crossover can be made within the formalism of the stream functions by reducing the droplet ellipticity ratio ξ_0 to zero value. However, the stability analysis indicates that the system starts to behave differently for the opposite direction of temperature gradient, $T_{dn} > T_{up}$. We reveal that the critical thermocapillary motion (with the positive ${\rm Ma}_c$ values) develops both in the ellipsoidal drop and in a flat liquid layer only when the hot fluid volume from the bottom surface with the sticking properties flows in the direction of the cold free surface (compare with [8,47]).

The predictions of our hydrodynamic theory can be checked using various experimental set ups. The experiments can be carried out both in the laboratory on the Earth and under microgravity conditions on the International Space Station. The geometry of the experiment with ellipsoidal fluid drops embedded in smectic films with asymmetric boundary conditions implies that the heat transfer occurs from the hot plate positioned at the upper side of the drop to the cold one placed at its bottom side. This corresponds to the positive direction of the temperature gradient ($T_{up} > T_{dn}$) (Fig. 4) and ensures that the buoyancy effects related to the convection in the surrounding air are absent.

The most important quantitative characteristic of the circulating Marangoni flow in the drops that can be directly measured in experiment is time period, Δt, i.e., the time interval required for the movement along the closed stream line. The time period can be defined as

$$\Delta t = \oint \frac{dl}{v}, \tag{84}$$

where v is a velocity modulus along the trajectory of the flow and dl is a tangential element of the curved trajectory, which

is determined as $dl_i = \sqrt{(x_{i+1} - x_i)^2 + (z_{i+1} - z_i)^2}$, where the set of points $\{(x_i, z_i)\}$ determines the velocity distribution within the drops and, accordingly, the streamlines. The magnitude of the circulation period Δt crucially depends on the values of Marangoni number, Ma, and the drop ellipticity ratio. As the flow velocity increases upon the Ma increase, the corresponding time period delta Δt diminishes. On the other hand, for the fixed values of Ma (i.e., of the temperature gradient across the drop) the length of the flattened circular trajectory increases upon the ellipticity ratio ξ_0 decrease. This leads to increase of the period of circulation Δt. The calculated values of Δt for the typical geometrical and material [72] parameters of the fluid drop are shown in the captions to Figs. 16 and 18. For example, for the velocity patterns shown in Fig. 18 the periods of circulation constitute 1.69, 1.95, 2.575, and 6.11 s counted off, respectively, from the center of vortex to its periphery. These time intervals are pretty large and can be registered by tracking the circulatory movement of the properly selected tracers within the drop.

VI. SUMMARY

In this work, we present a quantitative description of Marangoni flows in ellipsoidal isotropic droplets of different origin embedded in free-standing smectic films. The convection inside ellipsoidal fluid drops appears to be very different from the classical Marangoni convection in the systems with a simple flat geometry. In contrast to the flat fluid films, the mechanical equilibrium within drops is absent due to their curved shape. Because of the nonuniform temperature distribution the tangential Marangoni force activates a fluid flow along its curved interface, making the thermocapillary flow within the drop thresholdless. To describe the vortex formation in ellipsoidal isotropic droplets we generalized the method of the Stokes stream functions to the case of the curved fluid interfaces. It was shown that the general solution for the stream function can be represented as a sum over the limited amount of the basic functions which satisfy the boundary conditions of the problem and reflect the properties of the real physical fields. Moreover, we developed the original operator method for the solution of differential equations for the stream functions.

In general, the basic stream functions satisfy the symmetry of the problem and the condition of the absence of a fluid flow through the external drop boundary. Formally, this corresponds to the symmetrical case. As well we developed the straight method of obtaining the basic set of the stream functions describing thermocapillary flow in the drop for the asymmetric boundary conditions. In this case, the upper drop interface is connected with the air, while the bottom surface is in contact with the static smectic layers, so-called sticking or no-slip boundary conditions. To solve such a problem we represented the stream functions and the corresponding velocity components as a set of odd and even functions. The idea was to combine pairs of such functions to generate the basic set of the stream functions satisfying the sticking conditions at the bottom boundary of the drop. It is important that the basic stream functions (velocities) derived in this way provide a continuous variation through the points of contact between free and bounded by smectic layers surfaces of the drop. Next, we derived the distribution of temperature deviations inside the drop and in the ambient air. This allowed us, first, to resolve the Marangony boundary condition, and then to find the general solution for the stream functions and flow velocities, describing the stationary thermocapillary convection inside the drop with the actual temperature field within it taken into account. As a result, the general stream function and velocity fields, as well as the temperature distribution within ellipsoidal drops, were derived in the stationary regime for the fixed Marangoni numbers as a function of the droplet ellipticity ratio, and for the different values of the heat conductivity of the liquid crystal and air. In addition, numerical hydrodynamic calculations of the thermocapillary motion in ellipsoidal drops with asymmetric boundary conditions were carried out. Both the analytical and numerical simulations describe the axially symmetric circulatory convection flow induced by the thermocapillary effect at the droplet-free surface.

Finally, we note that the developed theory of Marangoni flow in droplets is quite general and, thus, can be applied to a wide variety of thermocapillary convection problems in fluid drops of the ellipsoidal form. As the first and foremost task we consider the Marangoni flows in isotropic ellipsoidal droplets suspended on the circular frame. The mechanical stability of such drops is determined by the sticking conditions at the solid bounding frame. The isotropic phase of various liquid crystal compounds, as well as the simple liquids of the type of glycerol or silicone oil can be considered for experimental and theoretical investigations. These droplets have a shape of the spherical segments (circular flat lenses), the height of which can vary relative to their lateral dimension by changing the amount of the material. As the second problem we indicate ellipsoidal nematic droplets spontaneously formed in overheated FSSFs. In this case, the FSSF of the appropriate material should be heated above the bulk smectic-nematic transition. There are also examples of the formation of fluid droplets of anisometric shape in various colloidal suspensions and among anisotropic fluids placed on a substrate with an ultra low wetting properties. Of special interest are also the thermocapillary processes in phospholipid membranes with various fluid inclusions, which can mimic the reaction of the cell membranes to the small temperature gradients.

ACKNOWLEDGMENTS

We are grateful to Vladimir V. Lebedev, Efim I. Kats, Igor V. Kolokolov, and Sergey S. Vergeles for fruitful discussions. We acknowledge support from the Russian Science Foundation (Grant No. 18-12-00108, general theory of Marangoni convection in isotropic drops embedded in free-standing films and corresponding numerical experiments). The work on the derivation of the stress tensor and expressions for the tangential forces in ellipsoidal coordinates and the elaboration of thermocapillary experiments was supported by the Russian Ministry of Science and Higher Education within the corresponding state assignments of FSRC "Crystallography and Photonics" RAS. The work on the problem statement, operator method and solving the problem of the temperature distribution within the ellipsoidal isotropic drops was supported by the Russian Ministry of Science and Higher

Education within the corresponding state assignments No. 0029-2019-0003.

E.S.P.: conceived the presented idea, calculated the Marangoni convection, solved the problem of the temperature distribution, discussed the results, wrote the final manuscript. M.A.S.: calculated the Marangoni convection, developed the original operator method for calculation of the stream functions, discussed the results. K.S.K.: made the numerical experiments, discussed the results. B.I.O: conceived of the presented idea, presentation of the results of the calculations, and elaboration of the thermocapillary experiments, discussed the results, and wrote the final manuscript. S.A.P.: conceived of the presented idea, worked on the derivation of the stress tensor and expressions for the tangential forces in ellipsoidal coordinates, contributed to the calculations, discussed the results. All authors read and agreed on the final text of the paper.

APPENDIX A: ELLIPSOIDAL COORDINATES AND DIFFERENTIATION OF UNIT VECTORS. BOUNDARY CONDITIONS

There are various methods of introducing of the ellipsoidal coordinates. The conventional approach consists in implementation of orthogonal coordinates α, β, φ which are useful to solve certain problems. The every point of space is described by a triple of numbers (α, β, φ), which correspond to an unique point in the Cartesian coordinates (x, y, z). The corresponding orthogonal system of surfaces consists of oblate spheroids formed by the surfaces of constant α ($\alpha = \alpha_0$ is the spheroid of the given boundary), one-sheeted hyperboloids of revolution of constant β, and planes of azimuthal angle φ = const [54,56], (compare with Fig. 2).

To solve the differential equations for the stream functions and to simplify the corresponding boundary conditions we prefer to use somewhat different representation of the orthogonal oblate spheroidal coordinates: $\xi = \sinh[\alpha]$, $u = \cos[\beta]$, $d\beta = -du/\sin[\beta]$, and φ. This corresponds to the new oblate spheroidal coordinates u, ξ, φ and the new right-hand triple of unit vectors $(\mathbf{e}_u, \mathbf{e}_\xi, \mathbf{e}_\varphi)$.

Let us define also the transformation relation for the differential operator ∇,

$$e^i_\mu \partial_i = \frac{1}{h_\mu}\partial_\mu, \tag{A1}$$

where indices i, μ correspond to Cartesian orthogonal coordinates and to oblate spheroidal coordinates, respectively; e^i_μ is the μ component of the unit vector in Cartesian coordinates.

Following Happel and Brenner, [56], we write the components of the unit vectors in oblate spheroidal coordinates and define the rule of differentiation of these unit vectors:

$$\mathbf{e}_\mu = \frac{1}{h_\mu}\partial_\mu x_i \mathbf{e}_i. \tag{A2}$$

For certain derivations we need to know the projections of the unit vectors on the z axis:

$$(e_z, \hat{\xi}) = \frac{1}{h_\xi}\partial_\xi z = \frac{c\,u}{h_\xi}, \tag{A3}$$

$$(e_z, \hat{u}) = \frac{1}{h_u}\partial_u z = \frac{c\,\xi}{h_u}, \tag{A4}$$

and on the radial axis:

$$(e_x, \hat{\xi}) = \frac{1}{h_\xi}\partial_\xi x = \frac{\xi\sqrt{1-u^2}}{\sqrt{\xi^2+u^2}}\cos[\varphi], \tag{A5}$$

$$(e_x, \hat{u}) = \frac{1}{h_u}\partial_u x = \frac{-u\sqrt{1+\xi^2}}{\sqrt{\xi^2+u^2}}\cos[\varphi]. \tag{A6}$$

The hybrid boundary conditions for the balance of tangential forces are given by the expressions

$$\hat{\sigma}_{\mu\alpha}\, n_\alpha = e^k_\mu e^i_\alpha \hat{\sigma}_{ik}\, n_\alpha = \eta\left[e^i_\mu \frac{\partial_\alpha}{h_\alpha}\left(e^i_\nu v_\nu\right) + e^k_\alpha \frac{\partial_\mu}{h_\mu}\left(e^k_\nu v_\nu\right)\right] n_\alpha$$

$$= \frac{1}{h_\mu}\partial_\mu \gamma \text{ (top surface)}, \tag{A7}$$

$$\hat{\sigma}_{\mu\alpha}\, n_\alpha = 0 \text{ (bottom surface)}. \tag{A8}$$

Because of $e^i_\mu e^i_\alpha = \delta_{\mu\alpha}$, $e^i_\mu e^k_\mu = \delta_{ik}$, and taking Eq. (A1) into account, the components of the unit vectors e^i_α in oblate spheroidal coordinates can be calculated using Eq. (A2).

APPENDIX B: STRAIGHT DERIVATION OF THE STREAM FUNCTIONS

In order to find the solution of Eq. (40) in ellipsoidal coordinates in terms of the stream functions it is important to know explicitly the properties of these functions. According to the definition of the stream function, $\psi = 0$ along the z axis, i.e., at $u = 1$ or $u = -1$. The solutions for ψ can be either symmetrical or asymmetrical with respect to variable u. This means that all solutions should be proportional either to $(1-u^2)$ or to $u\,(1-u^2)$.

Since $\psi(u = \pm 1) = 0$, any stream function can be expanded over a set of functions $\mathcal{F} = \int_{-1}^{u} P_n[u']\,du' = (P_{n+1} - P_{n-1})\,(2n+1)^{-1}$, i.e., $\psi = \sum_n \mathcal{F}_n(u) g_n(\xi)$, where $g_n(\xi)$ is an unknown function of ψ. According to the properties of Legendre polynomials, in order to find solutions for ψ with the accuracy up to u^4 or u^5 we should combine the solutions for stream function either symmetrical,

$$\psi_{ev} = \int_{-1}^{u} du P_3[u] g_3[\xi] + \int_{-1}^{u} du P_1[u] g_1[\xi], \tag{B1}$$

or asymmetrical with respect to u,

$$\psi_{\text{odd}} = \int_{-1}^{u} du P_4[u] g_4[\xi] + \int_{-1}^{u} du P_2[u] g_2[\xi]. \tag{B2}$$

In order to find the solutions for ψ with the higher accuracy up to u^{2m} or u^{2m+1} for $m > 2$, we should write the solution in the form of a sum of linearly independent terms proportional to integrals over Legendre polynomials of the higher order. For example, for symmetrical functions:

$$\psi^{(2m+1)}_{ev} = \int_{-1}^{u} du P_{2m+1}[u] g_{2m+1}[\xi] + \cdots + \int_{-1}^{u} du P_3[u] g_3[\xi] + \int_{-1}^{u} du P_1[u] g_1[\xi]. \tag{B3}$$

In accordance with Eqs. (B1)–(B3), the substitution for the stream function $\psi = f[u]\, g[\xi]$, can be used. Then the

equation $\Delta\psi = 0$ takes the form

$$\hat{\mathrm{E}}^2\psi = \frac{1}{c^2\,(u^2+\xi^2)}\big[f(u)\,(1+\xi^2)\,\partial_\xi^2 g(\xi) + g(\xi)\,(1-u^2)\,\partial_u^2 f(u)\big] = \frac{1}{c^2\,(u^2+\xi^2)}\,Y[u,\xi]. \tag{B4}$$

Accordingly, Eq. (33) can be rewritten as

$$c^4(\xi^2+u^2)^2\hat{\mathrm{E}}^4\psi = (1+\xi^2)\left\{\left[\frac{8\xi^2}{(u^2+\xi^2)^2} - \frac{2}{(u^2+\xi^2)}\right]Y - 2\frac{2\xi}{(u^2+\xi^2)}\partial_\xi Y + \partial_\xi^2 Y\right\} + (1-u^2)\left\{\left[\frac{8u^2}{(u^2+\xi^2)^2} - \frac{2}{(u^2+\xi^2)}\right]Y - 2\frac{2u}{(u^2+\xi^2)}\partial_u Y + \partial_u^2 Y\right\}. \tag{B5}$$

It is instructive to find the solutions of Eq. (B4) for the case (B2). For ψ_{odd}, Eq. (B4) takes the form

$$\hat{\mathrm{E}}^2\psi_{\mathrm{odd}} = \frac{u^2-1}{u^2+\xi^2}\Bigg(\underbrace{\frac{(\xi^2+1)g_1'' - 2g_1}{2}}_{G_1[\xi]} + \underbrace{\frac{(1+\xi^2)g_3'' - 12g_3}{8}}_{G_3[\xi]}(5u^2-1)\Bigg). \tag{B6}$$

In turn, Eq. (B5) can be written as

$$\hat{\mathrm{E}}^4\psi = \frac{u^2-1}{(u^2+\xi^2)^3}(u^4\,\Psi_4 + u^2\Psi_2 + \Psi_0) = 0, \tag{B7}$$

where the functions Ψ_2, Ψ_4, and Ψ_0 are conjugated with $\{u^4, u^2, 1\}$, respectively, and can be represented as

$$\Psi_4[\xi] = 5(1+\xi^2)\partial_\xi^2 G_3 - 10G_3 = 0\,, \tag{B8}$$

$$\Psi_2[\xi] = (1+\xi^2)\left(-20\xi^3\partial_\xi G_3 - \partial_\xi^2 G_3 + 5\xi^2\partial_\xi^2 G_3\right) - 30\xi^2 G_3 - 10G_3 + (1+\xi^2)\partial_\xi^2 G_1 = 0, \tag{B9}$$

$$\Psi_0[\xi] = (1+\xi^2)\left[\xi^2\left(\partial_\xi^2 G_1 - \partial_\xi^2 G_3\right) - 4\xi\,(\partial_\xi G_1 - \partial_\xi G_3)\right] + 4\,(1+\xi^2)G_1 - 4G_3 + 6\xi^2 G_3 = 0. \tag{B10}$$

Each of expressions (B8)–(B10) is equal to zero since the components of $\{u^4, u^2, 1\}$ are linearly independent. This allows us to obtain the triple set of corresponding differential equations. After solving Eqs. (B8)–(B10) and subsequent substitution of all boundary and regularity conditions we obtain the expression for ψ_{odd}.

APPENDIX C: DERIVATION OF THE BASIC FUNCTIONS OF LAPLACE EQUATION

The Laplace equation for the temperature distribution T within the drop in the oblate spheroid coordinates ξ, u, φ reads

$$\Delta T = \frac{c}{h_\xi h_u h_\varphi}\big[\partial_\xi(1+\xi^2)\partial_\xi + \partial_u(1-u^2)\partial_u + (\xi^2+u^2)\partial_\varphi^2\big]T = 0. \tag{C1}$$

To solve this equation the separation of the variables is used: $T[\xi,u,\varphi] = \Xi[\xi]U[u]\Phi[\varphi]$ [54–56], where $\Xi[\xi], U[u], \Phi[\varphi]$ are the functions of one single variable ξ, u, or φ, respectively; $\Phi = e^{im\varphi}$ for $m \in \mathbb{Z}$ due to continuity on $\varphi \in \mathbb{T}^1$. Due to an axial symmetry of the system $m = 0$, and for the function U we obtain the Legendre equation. As a result, the constant of separation is $n(n+1)$ and $U = U_n = P_n[u]$, where $P_n[u]$ is a Legendre polynomial of the first kind (the temperature T is supposed to be regular for all u). In turn, for Ξ, we obtain the equation

$$\partial_\xi(1+\xi^2)\partial_\xi\,\Xi_n - n(n+1)\Xi_n = 0, \tag{C2}$$

the first solution of which, $\Xi_n^{(1)}[\xi]$, is the Legendre polynomial of the first kind of the imaginary argument $P_n[I\xi]$ [54]. The exclusion of the imaginary part leads to the simple transformation rules:

$$\Xi_{2n}^{(1)}[\xi] = P_{2n}[i\xi], \tag{C3}$$

$$\Xi_{2n+1}^{(1)}[\xi] = (-i)P_{2n+1}[i\xi]. \tag{C4}$$

On the basis of these rules, we can use for $\Xi_n^{(1)}[\xi]$ the transformed recurrent relations for Legendre polynomials with the argument $z = i\xi$, in particular

$$(1-z^2)\,\frac{dP_n[z]}{dz} = n\,P_{n-1}[z] - n\,z\,P_n[z]. \tag{C5}$$

The latter can be transformed to

$$(1+\xi^2)\,\frac{d\,\Xi_{2n}^{(1)}[\xi]}{d\xi} = -2\,n\,\Xi_{2n-1}^{(1)}[\xi] + 2\,n\,\xi\,\Xi_{2n}^{(1)}[\xi], \tag{C6}$$

$$(1+\xi^2)\,\frac{d\,\Xi_{2n+1}^{(1)}[\xi]}{d\xi} = (2n+1)\,\Xi_{2n}^{(1)}[\xi] + (2n+1)\,\xi\,\Xi_{2n+1}^{(1)}[\xi]. \tag{C7}$$

Equation (C7) is a certain representation of the Legendre polynomial of the second kind. By disposing of the imaginary unit, we obtain directly $\Xi_0^{(1)}[\xi] = 1$, $\Xi_0^{(2)}[\xi] = \arctan[\xi]$, $\Xi_1^{(1)}[\xi] = \xi$, $\Xi_1^{(2)}[\xi] = \xi\,\arctan[\xi] + 1$; other solutions for Ξ_n $(n > 2)$ are obtained via the recurrent relation

$$\Xi_{n+1} = (-1)^n\frac{2n+1}{n+1}\,\xi\,\Xi_n - \frac{n}{n+1}\,\Xi_{n-1}. \tag{C8}$$

Using the recurrent relation (C8) we can write the successive expressions of $\Xi_n[\xi]$ for various n:

$$\begin{aligned}
&\Xi_0^{(1)}[\xi] = 1, \quad \Xi_0^{(2)}[\xi] = \arctan[\xi],\\
&\Xi_1^{(1)}[\xi] = \xi, \quad \Xi_1^{(2)}[\xi] = \xi\,\arctan[\xi] + 1,\\
&\Xi_2^{(1)}[\xi] = -\frac{1}{2} - \frac{3\xi^2}{2},\\
&\Xi_2^{(2)}[\xi] = -\frac{\arctan[\xi]}{2} - \frac{3}{2}\xi(1+\xi\,\arctan[\xi]),
\end{aligned} \tag{C9}$$

etc.

To find the temperature distribution in the air it is convenient to use the linear combinations of $\Xi_n^{(1,2)}$, damped at

$\xi \to +\infty$, designated below as $\Xi_n^{(a)}$:

$$\Xi_0^{(a)} = -\arctan[\xi] + \frac{\pi}{2},$$
$$\Xi_1^{(a)} = \xi \arctan[\xi] - \frac{\pi\xi}{2} - 1, \tag{C10}$$
$$\Xi_2^{(a)} = \frac{3\xi(2\xi \arctan[\xi] - \pi\xi + 2)}{4} + \frac{\arctan[\xi]}{2} - \frac{\pi}{4},$$

etc.

APPENDIX D: SOME ALGEBRAIC RELATIONS

We derive here some algebraic relations which are useful in calculation of the ψ functions.

$$\mathcal{F}_n = \int_{-1}^{u} P_n[u']\,du' = \frac{P_{n+1} - P_{n-1}}{2n+1}. \tag{D1}$$

After multiplying of the both sides of Eq. (D1) by u we obtain

$$u\mathcal{F}_n = \frac{n+2}{2n+1}\mathcal{F}_{n+1} + \frac{n-1}{2n+1}\mathcal{F}_{n-1}. \tag{D2}$$

After doing this for a second time we have

$$u^2\mathcal{F}_n = \frac{(n+2)(n+3)}{(2n+1)(2n+3)}\mathcal{F}_{n+2} + \left[\frac{n(n+2)}{(2n+1)(2n+3)} + \frac{(n-1)(n+1)}{(2n+1)(2n-1)}\right]\mathcal{F}_n + \frac{(n-1)(n-2)}{(2n+1)(2n-1)}\mathcal{F}_{n-2}. \tag{D3}$$

For the derivation of the temperature distribution within a drop it is useful to know the following equation:

$$u\partial_u\mathcal{F}_n = uP_n = \frac{n+1}{2n+1}P_{n+1} + \frac{n}{2n+1}P_{n-1}. \tag{D4}$$

To calculate the certain boundary conditions the following equations might be useful:

$$F_{ik} = \int_{-1}^{1} \mathcal{F}_i\mathcal{F}_k\frac{du}{1-u^2} = \delta_{ik}\frac{2}{i(i+1)(2i+1)}, \tag{D5}$$
$$\partial_u P_n = \frac{n}{1-u^2}(P_{n-1} - uP_n) = \frac{n}{1-u^2}\frac{n+1}{2n+1}(P_{n-1} - P_{n+1}) = -\frac{n(n+1)}{1-u^2}\mathcal{F}_n. \tag{D6}$$

APPENDIX E: DERIVATION OF STREAM FUNCTIONS

We introduce a number of operators which considerably simplify the calculations of the stream functions:

$$\hat{P} = \partial_u(1-u^2)\partial_u, \quad \hat{P}P_n = -n(n+1)P_n, \tag{E1}$$
$$\hat{\mathcal{F}} = (1-u^2)\partial_u^2, \quad \hat{\mathcal{F}}\mathcal{F}_n = -n(n+1)\mathcal{F}_n, \tag{E2}$$
$$\hat{\Xi} = \partial_\xi(1+\xi^2)\partial_\xi, \quad \hat{\Xi}\Xi_n = n(n+1)\Xi_n, \tag{E3}$$
$$\hat{\mathcal{X}} = (1+\xi^2)\partial_\xi^2, \quad \hat{\mathcal{X}}\mathcal{X}_n = n(n+1)\mathcal{X}_n, \tag{E4}$$

where the functions $\mathcal{X}_n$ are introduced similarly to $\mathcal{F}_n$,

$$\mathcal{X}_n = \frac{\Xi_{n+1} - \Xi_{n-1}}{2n+1}. \tag{E5}$$

Since $\psi(u = \pm 1) = 0$, any stream function can be expanded over a set of $\mathcal{F}$, i.e. $\psi = \sum_n \mathcal{F}_n[u]g_n[\xi]$, where $g_n[\xi]$ is an unknown function of ψ. The operator $\hat{E}^2$ acts on the monom $\mathcal{F}_n g_n$ as

$$\hat{E}^2\mathcal{F}_n g_n = \frac{\hat{\mathcal{X}} + \hat{\mathcal{F}}}{\xi^2+u^2}(\mathcal{F}_n g_n) = \frac{1}{\xi^2+u^2}\mathcal{F}_n\underbrace{[\hat{\mathcal{X}}g_n - n(n+1)g_n]}_{G_n}, \tag{E6}$$

where we define an unknown function $G_n[\xi]$. Let us note that the kernel of the operator $\hat{E}^2$ is $\{\mathcal{X}_n\mathcal{F}_n\}$ [see Eqs. (E2) and (E4)]. In turn, for the action of the operator $\hat{E}^4$ on the monom $\mathcal{F}_n g_n$ we obtain

$$\hat{E}^4\mathcal{F}_n g_n = \hat{E}^2\frac{1}{u^2+\xi^2}\mathcal{F}_n G_n = \frac{1}{\xi^2+u^2}(\hat{\mathcal{X}} + \hat{\mathcal{F}})\frac{1}{u^2+\xi^2}\mathcal{F}_n G_n. \tag{E7}$$

Let us derive the commutator

$$\left[\hat{\mathcal{F}}\frac{1}{\xi^2+u^2}\right] = \left[(1-u^2)\partial_u^2, \frac{1}{u^2+\xi^2}\right] = (1-u^2)\left[\partial_u^2, \frac{1}{\xi^2+u^2}\right] = (1-u^2)\left[\frac{-2(\xi^2+u^2)+8u^2}{(\xi^2+u^2)^3} + \frac{-4u}{(\xi^2+u^2)^2}\partial_u\right], \tag{E8}$$

with the help of which the required expression (E7) reads

$$\hat{E}^4\mathcal{F}_n g_n = \frac{1}{(\xi^2+u^2)^3}\{6(\xi^2-u^2) + 4 - 4[(1-u^2)u\partial_u + (1+\xi^2)\xi\partial_\xi] + (\xi^2+u^2)[\hat{\mathcal{X}} - n(n+1)]\}\mathcal{F}_n G_n. \tag{E9}$$

In order to expand expression (E9) over $\mathcal{F}_m$ we should know how the operator $u(1-u^2)\partial_u$ acts on this function:

$$u(1-u^2)\partial_u\mathcal{F}_n = -\frac{(n+1)(n+2)(n+3)}{(2n+1)(2n+3)}\mathcal{F}_{n+2} + \left[-\frac{n(n+1)(n+2)}{(2n+1)(2n+3)} + \frac{n(n+1)(n-1)}{(2n+1)(2n-1)}\right]\mathcal{F}_n + \frac{n(n-1)(n-2)}{(2n+1)(2n-1)}\mathcal{F}_{n-2}. \tag{E10}$$

Finally, we arrive at

$$(\xi^2+u^2)^3\hat{E}^4\mathcal{F}_n g_n = \mathcal{F}_{n+2}\hat{U}_n G_n + \mathcal{F}_n\hat{S}_n G_n + \mathcal{F}_{n-2}\hat{\mathcal{D}}_n G_n, \tag{E11}$$

where

$$\hat{U}_n = \frac{(n+2)(n+3)}{(2n+1)(2n+3)}[\hat{\mathcal{X}} - (n-2)(n-1)], \tag{E12}$$
$$\hat{S}_n = 6\xi^2 + 4 - 4\xi(1+\xi^2)\partial_\xi + \xi^2[\hat{\mathcal{X}} - n(n+1)] + \frac{n(n+2)}{(2n+1)(2n+3)}[\hat{\mathcal{X}} - (n-2)(n-1)]$$

$$+\frac{(n-1)(n+1)}{(2n+1)(2n-1)}[\hat{\mathcal{X}}-(n+2)(n+3)], \quad \text{(E13)}$$

$$\hat{\mathcal{D}}_n=\frac{(n-1)(n-2)}{(2n+1)(2n-1)}[\hat{\mathcal{X}}-(n+2)(n+3)]. \quad \text{(E14)}$$

Let us consider the representation $\psi_N^{(p)}=\mathcal{F}_N g_N+\mathcal{F}_{N-2}g_{N-2}$, $(N>2)$, for the solutions of Eq. (40) for ψ, which does not include the kernel of the operator $\hat{E}^2$. Then it follows from Eqs. (E4) and (E12) that for the contribution proportional to $\mathcal{F}_{N+2}$ in Eq. (E11) to be equal to zero, the following equation should be fulfilled:

$$G_N=\mathcal{X}_{N-2}. \quad \text{(E15)}$$

In this case to obtain the zero coefficient at $\mathcal{F}_N$ in Eq. (E11) the following equality should hold:

$$-\hat{U}_{N-2}G_{N-2}=\hat{S}_N\mathcal{X}_{N-2}. \quad \text{(E16)}$$

In turn, using Eqs. (C3)–(C8), (E4), and (E13), we find

$$\begin{aligned}\hat{S}_N\mathcal{X}_{N-2}=&\left\{6\xi^2+4-4\xi(1+\xi^2)\partial_\xi+\xi^2[\hat{\mathcal{X}}-N(N+1)]\right.\\&\left.+\frac{(N-1)(N+1)}{(2N+1)(2N-1)}[\hat{\mathcal{X}}-(N+2)(N+3)]\right\}\mathcal{X}_{N-2}\\=&\frac{4N(N+1)}{(2N-1)}\mathcal{X}_N. \quad \text{(E17)}\end{aligned}$$

By means of simple algebra, we obtain from Eq. (E16), using Eqs. (E12) and (E17) $[\hat{\mathcal{X}}-(N-4)(N-3)]G_{N-2}=-4(2N-3)\mathcal{X}_{\mathcal{N}}$, which leads to

$$\hat{G}_{N-2}=-\mathcal{X}_N. \quad \text{(E18)}$$

After substitution of the expressions for G_N, G_{N-2} [(E15) and (E18)] in Eqs. (E11)–(E14) one can see that multiplier at $\mathcal{F}_{N-2}$ is equal to zero, $\hat{\mathcal{D}}_{N-2}G_{N-2}=0$, and $\hat{\mathcal{D}}_N G_N=-\hat{S}_{N-2}G_{N-2}$. This means that these terms cancel out each other in Eq. (E11).

Thus the final representation of the partial solution for the stream function $\psi_{N>2}^{(p)}$ (i.e., $\psi_{N>2}$ without the contribution of the kernel of operator $\hat{E}^2$) is

$$\psi_{N>2}^{(p)}=\mathcal{F}_N\mathcal{X}_{N-2}+\mathcal{F}_{N-2}\mathcal{X}_N. \quad \text{(E19)}$$

Let us consider the partial solutions for $\psi_{N\leqslant 2}^{(p)}$ separately:

$N=1$: In this case $\psi_1^{(p)}=\mathcal{F}_1 g_1$, in turn, $\hat{\mathcal{D}}_1=0$, and for the equality $\hat{U}_1G_1=0$ to be satisfied, the fulfillment of the equality $\hat{\mathcal{X}}G_1=0$ is necessary; at the same time $\hat{S}_1G_1=0\Rightarrow G_1\propto\xi$, $(\hat{\mathcal{X}}-2)g_1=\xi$, that leads to the relation $g_1\propto\xi$.

$N=2$: In this case $\psi_2^{(p)}=\mathcal{F}_2 g_2$, $\hat{\mathcal{D}}_2=0$, $\hat{\mathcal{X}}G_2=0$, $\hat{S}_2G_2=0\Rightarrow G_2\propto 1$, $(\hat{\mathcal{X}}-3)g_2=1$, i.e., $g_2\propto 1$.

As a result, we arrive to the full solution of Eq. (40) for the stream function ψ, which is a combination of the stream functions $\psi_{1,2}^{(p)}$, $\psi_N^{(p)(1,2)}$ and of the kernel of operator $\hat{E}^2$:

$$\begin{aligned}\psi=&c_1\xi\mathcal{F}_1+c_2\mathcal{F}_2+\sum_{N>2}c_N^{(1)}\left(\mathcal{F}_N\mathcal{X}_{N-2}^{(1)}+\mathcal{F}_{N-2}\mathcal{X}_N^{(1)}\right)\\&+c_N^{(2)}\left(\mathcal{F}_N\mathcal{X}_{N-2}^{(2)}+\mathcal{F}_{N-2}\mathcal{X}_N^{(2)}\right)\\&+\sum_{N\geqslant 1}c_{No}^{(1)}\mathcal{X}_N^{(1)}\mathcal{F}_N+c_{N\mathcal{K}}^{(2)}\mathcal{X}_N^{(2)}\mathcal{F}_N. \quad \text{(E20)}\end{aligned}$$

For the problem under consideration we are interested in the continuously differentiable (smooth) solutions for the stream function inside an oblate spheroid. In accordance with the general rule, for such solutions the same evenness over u and ξ should be fulfilled (in this case the solution is automatically regular at $\xi=u=0$; see Sec. I A). This leads to $\{c_1, c_2, c_N^{(2)}, c_{N\mathcal{K}}^{(2)}\}=0$.

Finally, the necessary smooth solution of Eq. (40) for the stream function has the form

$$\psi=\sum_{N>2}c_N\,\psi_N, \quad \text{(E21)}$$

where basic functions ψ_N can be written as

$$\psi_N=\mathcal{F}_N\left(\mathcal{X}_{N-2}^{(1)}+c_{N\mathcal{K}}\,\mathcal{X}_N^{(1)}\right)+\mathcal{F}_{N-2}\left(\mathcal{X}_N^{(1)}+\widetilde{c}_{N\mathcal{K}}\,\mathcal{X}_{N-2}^{(1)}\right). \quad \text{(E22)}$$

In turn, the constants $c_{N\mathcal{K}}$, $\widetilde{c}_{N\mathcal{K}}$ can be found from the condition $\psi(\xi=\xi_0)=0$:

$$c_{N\mathcal{K}}=-\frac{\mathcal{X}_{N-2}^{(1)}(\xi_0)}{\mathcal{X}_N^{(1)}(\xi_0)}, \quad \widetilde{c}_{N\mathcal{K}}=-\frac{\mathcal{X}_N^{(1)}(\xi_0)}{\mathcal{X}_{N-2}^{(1)}(\xi_0)}=\frac{1}{c_{N\mathcal{K}}}. \quad \text{(E23)}$$

The expression (E22) is used in our analytical calculations [see, for example, Eq. (42)].

APPENDIX F: DETAILS OF CALCULATIONS OF THE BASIC STREAM FUNCTIONS. GENERAL STATIONARY SOLUTIONS AND CRITICAL VALUES OF MA

1. Derivation of the basic set $\{\psi_{j,st}\}$

Here we present the details of derivation of the basic set of the stream functions $\{\psi_{j,st}\}$ for the case of the sticking boundary conditions at the bottom drop surface. In doing so we use the basic stream functions $\psi_j[\xi,u]$ and introduce the corresponding tangential velocity component $v_{u,j}[\xi,u]$ for odd and even functions over the variable u: $\psi_j^{\rm odd}$, ψ_j^{ev}, $v_{u,j}^{\rm odd}$, $v_{u,j}^{ev}$. To build up the new basic stream functions which satisfy the sticking boundary condition we are using the following mathematical trick. We start with the expansion of the partial derivative $\partial_\xi\psi_l^{\rm odd}[\xi=\xi_0,|u|]$ at $\xi=\xi_0$ over the set of functions $\partial_\xi\psi_j[\xi=\xi_0,u]$,

$$\partial_\xi\psi_l^{\rm odd}[\xi=\xi_0,|u|]=\sum_{j_{\rm even}}c_{lj}\,\partial_\xi\psi_j[\xi=\xi_0,u], \quad \text{(F1)}$$

which leads to the equality

$$\underbrace{\partial_\xi\left(\psi_l^{\rm odd}+\sum_{j_{\rm even}}c_{jl}\,\psi_j\right)}_{\psi_{l,st}}[\xi=\xi_0]=0 \quad \text{for } u<0. \quad \text{(F2)}$$

The above equations provide us with a set of functions $\psi_l^{\rm odd}$ which allows us to generate the full basis $\{\psi_{j,st}\}$.

The desired basis provides equation $\partial_\xi\psi_l^{\rm odd}[|u|]|_{\xi=\xi_0}=\hat{O}_{il}^{\rm stick}\mathcal{F}_i[|u|]$, where the matrix $\hat{O}_{il}^{\rm stick}$ describes the action of the operator ∂_ξ on the expansion of the stream function $\psi_l^{\rm odd}[\xi,u]$ at $\xi=\xi_0$. For the implementation of the above procedure it is necessary to obtain an expansion of the symmetrized function $\mathcal{F}_i[|u|]$ over a set of functions $\{\mathcal{F}_m\}$:

$$\mathcal{F}_i[|u|]=k_{im}\mathcal{F}_m. \quad \text{(F3)}$$

The corresponding coefficients k_{im} can be calculated by means of Eq. (D6), taking the orthogonality of the functions $\mathcal{F}_m$ in the interval $[-1, 1]$ into account [see Eq. (D1)]:

$$k_{im} = P_i[0](P_{m+1}[0] - P_{m-1}[0])\,\frac{m(m+1)}{i(i+1) - m(m+1)}. \quad \text{(F4)}$$

In order to calculate the coefficients c_{jl} in the expansion of the stream function ψ_l^{odd} over the function ψ_j^{even} it is necessary to invert the matrix $\hat{O}_{mj}^{\text{stick}}$ which leads to the following equation:

$$\sum_{j_{\text{even}}} \hat{O}_{mj}^{\text{stick}} c_{jl} = \sum_i k_{im} \hat{O}_{il}^{\text{stick}}. \quad \text{(F5)}$$

Equation (F5) can be solved explicitly because in accordance with expression (42) the matrix $\hat{O}_{mj}^{\text{stick}}$ is a lower triangular matrix [see Eq. (E22)].

2. Validation of the condition $n \neq k$

The next point that should be clarified is a justification of the condition $n \neq k$ in Eq. (60). Let us note, that for the response to the right part of Eqs. (57)–(59) the condition $n \neq k$ is valid due to the explicit form of the solution for v_z, as each ψ_n from the obtained set $\{\psi_j\}$ has contributions of the form $\mathcal{F}_n\mathcal{X}_n$ and $\mathcal{F}_n\mathcal{X}_{n-2} + \mathcal{F}_{n-2}\mathcal{X}_n$ [see Eqs. (42)–(44) and (C8)–(C10)]:

$$v_z[\psi = \mathcal{F}_n\mathcal{X}_n] = -\frac{P_{n+1}\,\Xi_{n-1} - P_{n-1}\,\Xi_{n+1}}{2n+1}, \quad \text{(F6)}$$

$$\begin{aligned} v_z[\psi = \mathcal{F}_n\mathcal{X}_{n-2} + \mathcal{F}_{n-2}\mathcal{X}_n] = {} & 2\,\frac{P_{n+1}\,\Xi_{n-1} - \Xi_{n+1}P_{n-1}}{(2n-3)(2n+1)} \\ & - \frac{2n-1}{(2n+1)(2n-3)}(P_{n+1}\,\Xi_{n-3} - P_{n-3}\,\Xi_{n+1}) \\ & - 2\,\frac{P_{n-1}\,\Xi_{n-3} - P_{n-3}\,\Xi_{n-1}}{(2n+1)(2n-3)}. \end{aligned} \quad \text{(F7)}$$

In other words, in the right part of Eq. (59) the functions $P_n(u)$ are always multiplied by $\Xi_k^{(1)}$ with $n \neq k$.

3. Derivation of the general stream function through the basic set $\psi_{i,st}$

In order to derive the general stream function we need to know the coefficients $c_{i,st}$ of the expansion of the full stream function over basic functions $\psi_{i,st}$ [see Eq. (69)] . We search for the finite approximation of this solution. The series is broken once the following convergence criterion is satisfied: the norm of deviation from the required equation (74), given by Eq. (75), should be minimal for the derived N_r-measured set of $c_{i,st}$,

$$\begin{aligned} E[\{c_{j,st}\}] = {} & c_{j,st}c_{m,st} \underbrace{\sum_{i,l} \int \hat{O}_{ij}^{\text{free}} \mathcal{F}_i \hat{O}_{lm}^{\text{free}} \mathcal{F}_l \frac{du}{1-u^2}}_{\hat{M}_{jm}} \\ & - 2\,c_{j,st} \underbrace{\sum_{i} \int \hat{O}_{ij}^{\text{free}} \mathcal{F}_i\, r[u] \frac{du}{1-u^2}}_{\mathcal{R}_j} \\ & + \int (r[u])^2 \frac{du}{1-u^2} \;\rightarrow\; \delta E{=}0 \Rightarrow \hat{M}_{mj} c_{j,st}^{(\text{opt})} {=} \mathcal{R}_m. \end{aligned} \quad \text{(F8)}$$

In this way the optimal solution for a set $\{c_{j,st}\}$ can be calculated with the given accuracy.

4. Details of calculations of the critical Marangoni number Ma_c

In this subsection we present the details of finding of the solution of Eq. (83). The standard method to obtain the solution of Eq. (83) is its reduction to the generalized eigenvalue problem:

$$\hat{\mathcal{A}} - \text{Ma}_c\hat{\mathcal{B}} = \begin{pmatrix} \hat{M}_0 & 0 \\ 0 & \hat{I} \end{pmatrix} - \text{Ma}_c \begin{pmatrix} \hat{M}_1 & -\hat{M}_2 \\ \hat{I} & 0 \end{pmatrix}, \quad \text{(F9)}$$

$$|\mathcal{V}\rangle = \begin{pmatrix} |c_c\rangle \\ \text{Ma}_c|c_c\rangle \end{pmatrix} \;\rightarrow\; (\hat{\mathcal{A}} - \text{Ma}_c\hat{\mathcal{B}})|\mathcal{V}\rangle = 0, \quad \text{(F10)}$$

where matrices $\hat{M}^{(0)}, \hat{M}^{(1)}, \hat{M}^{(2)}$ are determined in expression (82) as interlinear (footnote) designations, and matrices $\hat{\mathcal{A}}, \hat{\mathcal{B}}$ are obtained from Eq. (83) through $\hat{M}^{(0)}, \hat{M}^{(1)}, \hat{M}^{(2)}$, and $|\mathcal{V}\rangle$ is the unknown eigenvector of the matrix $(\hat{\mathcal{A}} - \text{Ma}_c\hat{\mathcal{B}})$. Because the quadratic eigenvalue problem is well known, there are reliable methods of its solution [74].

APPENDIX G: NUMERICAL SIMULATION

1. Formulation of the problem

An isotropic liquid droplet in the form of an oblate spheroid formed in the free-standing smectic film (FSSF) is placed inside a cylindrical chamber between two round plates with different temperatures: T_{up} is the top plate temperature and T_{dn} is the bottom plate temperature. The drop is in the ambient air at the normal atmospheric pressure. A thin smectic film of uniform thickness keeps the droplet in horizontal plane at the same distance from each plate. The edges of the FSSF are connected with a rigid frame which is attached to the side wall of the cylindrical chamber. We assume that the geometry of the droplet and film does not change over time. Since the thickness of the smectic film is much less than the thickness of the isotropic liquid drop, we do not take the thermal properties of the FSSF into account.

The side wall of the chamber is made of the thermal insulating material; therefore, we do not take into account the heat exchange of our system with the environment. The transfer of heat in the air occurs due to the thermal conductivity. The convection and radiation are not taken into account. The heat transfer in the droplet occurs due to the thermal conductivity and convection. Since the thickness of the drop in the vertical direction is much less than along the horizontal, we do not take into account the flows in the bulk caused by the difference in the density of the liquid due to the spatial inhomogeneity of the temperature field. We consider only the thermocapillary flow of liquid, which arises due to the dependence of the surface tension of fluid on temperature. This type of convection within the liquid is known as the Marangoni flow. The physical and geometric parameters of the problem are presented in Table I. We take into account the linear dependence of the surface tension of fluid on temperature, $\gamma(T) = \gamma_0 - \varsigma(T - T_0)$, where γ_0 is the surface tension at the temperature $T = T_0$.

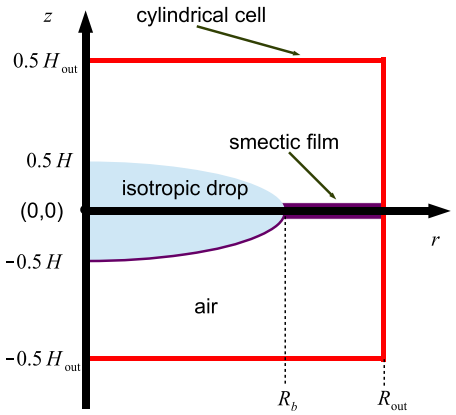

FIG. 29. Sketch for the problem statement: smectic film is at the bottom drop surface.

2. Mathematical model

Let the z axis corresponds to the axis of symmetry of the cylindrical chamber and of the droplet in the form of an oblate spheroid (see Fig. 29). We use here the cylindrical coordinates (r, φ, z). The zero of the z-coordinate axis is in the center of the drop. The center of the droplet and the chamber in the horizontal plane corresponds to the radial coordinate $r = 0$. The maximum droplet radius in the horizontal plane and the maximum droplet height in the vertical plane are R_b and H, respectively. The height and the radius of the cylindrical chamber are indicated as H_{out} and R_{out} (see Table I). In the problem under consideration, the transfer of mass and heat does not depend on the angular coordinate φ. This allows us to consider our problem as a two-dimensional one in the coordinates (r, z). In this formulation, the geometry of the droplet is described by an ellipse with a semimajor axis $a = R_b$, and a semiminor axis $b = 0.5H$.

The hydrodynamics within the droplet in the scheme under discussion is described as follows. First, we introduce the stream function ψ and the vorticity $\omega = \partial u/\partial z - \partial v/\partial r$, using the cylindrical coordinates [56]. Here u is the horizontal component of the liquid flow velocity vector, and v is the vertical component of this vector. Then, in accordance with [25,56,70] the vorticity transfer equation can be written as

$$\frac{\partial \omega}{\partial t} + u\frac{\partial \omega}{\partial r} + v\frac{\partial \omega}{\partial z} - \frac{u\omega}{r} = \frac{\eta}{\rho}\left[\frac{\partial^2 \omega}{\partial z^2} + \frac{1}{r}\frac{\partial}{\partial r}\left(r\frac{\partial \omega}{\partial r}\right) - \frac{\omega}{r^2}\right], \tag{G1}$$

where $u = (\partial\psi/\partial z)/r$, $v = -(\partial\psi/\partial r)/r$. Rewriting the expression for the vortex $\omega = \partial u/\partial z - \partial v/\partial r$ and using the stream function, the following equation is obtained [25,56]:

$$\frac{\partial^2 \psi}{\partial r^2} - \frac{1}{r}\frac{\partial \psi}{\partial r} + \frac{\partial^2 \psi}{\partial z^2} = r\omega. \tag{G2}$$

The temperature field T in the system is described by the heat transfer equation

$$\frac{\partial T}{\partial t} + \epsilon\left(u\frac{\partial T}{\partial r} + v\frac{\partial T}{\partial z}\right) = \frac{1}{c_p^{(g)}\rho^{(g)}}\left[\frac{\partial}{\partial z}\left(\varkappa^{(g)}\frac{\partial T}{\partial z}\right) + \frac{1}{r}\frac{\partial}{\partial r}\left(\varkappa^{(g)} r\frac{\partial T}{\partial r}\right)\right], \tag{G3}$$

where

$$\epsilon, c_p^{(g)}, \rho^{(g)}, \varkappa^{(g)} = \begin{cases} 1, c_p, \rho, \varkappa : & h_- < z < h_+, \\ 0, c_a, \rho_a, \varkappa_a : & |z| > h_+. \end{cases}$$

Here $c_p^{(g)}$, $\rho^{(g)}$, $\varkappa^{(g)}$ are the general notations for the specific heat capacity, density and thermal conductivity, respectively. The index a indicates the relation of the material parameter to the air. The parameter ϵ allows us to turn off the convective term in the air area. As a result, the heat transfer equation (G3) becomes the heat equation at $\epsilon = 0$. The droplet surface shape h is determined using canonical equation of the ellipse, $h_\pm = \pm b\sqrt{1 - (r/a)^2}$. For the case of a droplet in the form of a lens, we use two spherical segments attached to each other by their bases. From the canonical equation of a circle, we obtain the shape of the droplet surface $h_\pm = \pm\sqrt{R^2 - r^2} \mp (R - 0.5H)$, where the circle radius $R = [R_b^2 + (0.5H)^2]/H$. We also consider the case when the shape of the liquid corresponds to the lens with the truncated ends at the point $r = R_b - \delta r$. For definiteness, let us take the value $\delta r = 0.1R_b$.

Finally, we obtain the system of equations that includes Eqs. (G1)–(G3). The model consists of the three equations with the three variables to be found: ω, ψ, and T.

3. Initial and boundary conditions

At the initial time, the temperature in the system is uniform, $T(r, z, t = 0) = T_{\text{up}}$, and there are no liquid flows, $\omega(r, z, t = 0) = 0$. The value of the top plate temperature is the constant, $T(r, z = 0.5H_{\text{out}}, t) = T_{\text{up}}$. The bottom plate cools down to its stationary temperature T_{dn} in a relatively short period of time t_{rel}, $T(r, z = -0.5H_{\text{out}}, t) = T_{\text{up}} + (T_{\text{dn}} - T_{\text{up}})U_r(t)$, where

$$U_r(t) = \begin{cases} t/t_{\text{rel}}, & t \leqslant t_{\text{rel}}, \\ 1, & t > t_{\text{rel}}. \end{cases}$$

The heat relaxation time in the air is due to thermal conductivity, $t_{\text{rel}} = H_{\text{out}}^2 c_a \rho_a/\varkappa_a$. For the side wall of the chamber we use the condition of the heat flux absence, $\partial T(r = R_{\text{out}}, z, t)/\partial r = 0$. At the liquid-air boundary, the condition of equality of the temperatures and heat fluxes directed along the normal to this boundary should be satisfied. As indicated earlier, we do not take into account the thin smectic film. At $r = 0$, due to the axial symmetry of the system, the conditions $\partial T/\partial r = 0$, $\omega = 0$, $\psi = 0$ are held. At the liquid-air boundary we use the condition $\psi(r, z = h_\pm, t) = 0$, which follows from the impermeability condition. The normal vector $\mathbf{n}$ is directed outside the area with the liquid phase. The tangent vector $\boldsymbol{\tau}$ points to the right when viewed along the normal direction. For Marangoni flow to occur, it is necessary to fulfill the condition on the free surface of the droplet $\omega = \eta^{-1} d\gamma/d\tau + 2v_\tau d\theta/d\tau$, where $d\gamma/d\tau = -\varsigma\partial T/\partial\tau$ is the derivative of the surface tension along the tangent to the surface, v_τ is the tangential flow velocity, and θ is the angle between the tangent to the droplet surface and abscissa [25]. We express the tangential velocity as $v_\tau = u\cos\theta - v\sin\theta$, where $\cos\theta = \text{sgn}[z]/\sqrt{1 + (dh/dr)^2}$ and $\sin\theta = |dh/dr|/\sqrt{1 + (dh/dr)^2}$. We use also the geometrical relation $d\theta/d\tau = |d^2h/dr^2|[1 + (dh/dr)^2]^{-3/2}$ derived in

[25]. The tangential derivative of the temperature is found as $\partial T/\partial\tau = \cos\theta\,\partial T/\partial r - \sin\theta\,\partial T/\partial z$.

In the case when the surface of the droplet is covered with a layer of smectic, the no-slip condition is fulfilled, since the smectic is assumed to be immobile. This results in $v_\tau = 0$. The implementation of this condition at one of the drop interfaces is discussed in the next section.

4. Nondimensional formulation of the problem

Let us introduce the scaled quantities: characteristic length $l_c = H_{\text{out}}$, characteristic velocity $v_c = \eta/(\rho l_c)$, characteristic temperature $T_c = T_{\text{up}}$, characteristic thermal conductivity $\varkappa_c = \varkappa_a$, and characteristic time $t_c = l_c/v_c$. Further we use the relations $r = \tilde{r} l_c$, $z = \tilde{z} l_c$, $t = \tilde{t} t_c$, $u = \tilde{u} v_c$, $v = \tilde{v} v_c$, $\omega = \tilde{\omega} v_c/l_c$, $T = \tilde{T} T_c$, $\varkappa = \tilde{\varkappa}\varkappa_c$, $\varkappa_a = \tilde{\varkappa}_a\varkappa_c$, $\psi = \tilde{\psi} v_c l_c^2$. Here the tilde symbol indicates a dimensionless quantity. In all formulas, we use the dimensionless quantities and omit the tilde symbol for the brevity sake. The heat transfer equation (G3) in the dimensionless form reads

$$\frac{\partial T}{\partial t} + \epsilon\left(u\frac{\partial T}{\partial r} + v\frac{\partial T}{\partial z}\right) = \frac{1}{\text{Pe}}\left[\frac{\partial}{\partial z}\left(\varkappa^{(g)}\frac{\partial T}{\partial z}\right) + \frac{1}{r}\frac{\partial}{\partial r}\left(\varkappa^{(g)} r\frac{\partial T}{\partial r}\right)\right],$$

where the Péclet number is written as

$$\text{Pe} = \begin{cases} l_c^2 c_p \rho/(t_c\varkappa_c), & h_- < z < h_+, \\ l_c^2 c_a \rho_a/(t_c\varkappa_c), & |z| > h_+. \end{cases}$$

The boundary condition for the vorticity on the free liquid surface is now written as $\omega = 2v_\tau\, d\theta/d\tau - \text{Ma}'\, dT/d\tau$, where the modified Marangoni number is $\text{Ma}' = \varsigma T_c \rho l_c/\eta^2 \approx 200$. The use of the upper plate temperature as a characteristic scale is a forced necessity associated with computational difficulties. For comparison, the Marangoni number from the analytical part of the work is $\text{Ma} = \varsigma H^2(\Delta T/H_{\text{out}})c_p\rho/(\varkappa\eta) \approx 1$, where $\Delta T = |T_{\text{up}} - T_{\text{dn}}|$. For this reason, it is more convenient to make a comparison using the parameter $\Delta T/H_{\text{out}} = 10^4$ K/m.

On the boundary where the surface of the droplet is covered with a smectic, we use the condition $\partial\omega/\partial n = -\bar{q}\,\text{rot}_\tau\psi$, where the penalty parameter $\bar{q}$ is some relatively large number.

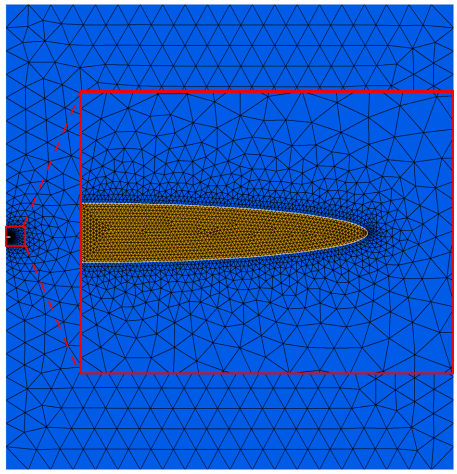

FIG. 30. Discretization of the spatial domain (the mesh used).

The derivative with respect to the normal is recorded on the left. This condition leads to the situation when $v_\tau \approx 0$ with a properly chosen value of the parameter $\bar{q}$. This allows us to mimic the no-slip condition. The dimensionless form of Eqs. (G1) and (G2) and other conditions (see Appendix G 3) does not differ from their dimensional form.

5. Numerical method

The problem, Eqs. (G1)–(G3) and conditions from Appendix G 3 in dimensionless forms, were solved using the commercial package FlexPDE Professional Version 7.18/W64 3D [75], the algorithm of which was implemented on the basis of the Galerkin finite element method. At each time step the modified iterative Newton-Raphson method is used [76]. The size of each time step in the program is determined automatically in order to minimize the calculation error. The mesh convergence of the problem solution is checked. The size of the mesh cells in the area of the droplet periodically decreased until the maximum flow velocity ceased to change. We settled on the mesh that included 2844 nodes and 5550 cells (Fig. 30).

[1] H. Bénard, Rev. Gén. des Sci. Pures et Appl. **11**, 1261 (1900).
[2] E. L. Koschmieder, Adv. Chem. Phys. **26**, 177 (1974).
[3] S. H. Davis, Annu. Rev. Fluid Mech. **19**, 403 (1987).
[4] E. L. Koschmieder and D. W. Switzer, J. Fluid Mech. **240**, 533 (1992).
[5] S. J. VanHook, M. F. Schatz, J. B. Swift, W. D. McCormick, and H. L. Swinney, J. Fluid Mech. **345**, 45 (1997).
[6] A. Alexeev, T. Gambaryan-Roisman, and P. Stephan, Phys. Fluids **17**, 062106 (2005).
[7] V. G. Levich, *Physicochemical Hydrodynamics* (Prentice-Hall, London, 1962).
[8] G. Z. Gershuni and E. M. Zhukhovitskii, *Convective Stability of an Incompressible Fluid* (Nauka, Moscow, 1972).
[9] A. V. Getling, Sov. Phys. Usp. **34**, 737 (1991).
[10] T. Gambaryan-Roisman, Adv. Colloid Interface Sci. **222**, 319 (2015).
[11] K. S. Kolegov and L. Yu. Barash, Adv. Colloid Interface Sci. **285**, 102271 (2020).
[12] M. A. Al-Muzaiqer, K. S. Kolegov, N. A. Ivanova, and V. M. Fliagin, Phys. Fluids **33**, 092101 (2021).
[13] L. A. Dávalos-Orozco, Microgravity Sci. Tech. **32**, 105 (2020).
[14] D. E. Melnikov, V. Shevtsova, T. Yano, and K. Nishino, Int. J. Heat Mass Transf. **87**, 119 (2015).
[15] T. Yano, K. Nishino, S. Matsumoto, I. Ueno, A. Komiya, Y. Kamotani, and N. Imaishi, Microgravity Sci. Technol. **30**, 599 (2018).
[16] K. Nakamura, H. N. Yoshikawa, Y. Tasaka, and Y. Murai, Phys. Rev. E **102**, 053102 (2020).

[17] J. Yoshioka, T. Sakikawa, Y. Ito, and K. Fukao, Phys. Rev. E **105**, L012701 (2022).

[18] M. Bestehorn, A. Pototsky, and U. Thiele, Eur. Phys. J. B **33**, 457 (2003).

[19] G. Wang, ASME J. Fluids Eng. **124**, 584 (2002).

[20] G. P. Sasmal and J. I. Hochstei, ASME J. Fluids Eng. **116**, 577 (1994).

[21] H. Hu and R. G. Larson, Langmuir **21**, 3972 (2005).

[22] H. Hu and R. G. Larson, J. Phys. Chem. B **110**, 7090 (2006).

[23] F. Girard, M. Antoni, S. Faure, and A. Steinchen, Langmuir **22**, 11085 (2006).

[24] D. Tam, V. von Arnim, G. H. McKinley, and A. E. Hosoi, J. Fluid Mech. **624**, 101 (2009).

[25] L. Yu. Barash, T. P. Bigioni, V. M. Vinokur, and L. N. Shchur, Phys. Rev. E **79**, 046301 (2009).

[26] W. D. Ristenpart, P. G. Kim, C. Domingues, J. Wan, and H. A. Stone, Phys. Rev. Lett. **99**, 234502 (2007).

[27] Y. Kita, A. Askounis, M. Kohno, Y. Takata, J. Kim, and K. Sefiane, Appl. Phys. Lett. **109**, 171602 (2016).

[28] Ch. Bohley and R. Stannarius, Soft Matter **4**, 683 (2008)

[29] S. Dölle, Z. Qi, C. S. Park, J. E. Maclennan, M. A. Glaser, N. A. Clark, K. Harth, and R. Stannarius, *Book of Abstracts of 41st German Conference on Liquid Crystals* (the University of Magdeburg, 2014), p. 29.

[30] Z. Qi, C. S. Park, M. A. Glaser, J. E. Maclennan, and N. A. Clark, Phys. Rev. E **93**, 012706 (2016).

[31] P. Oswald and P. Pierański, *Smectic and Columnar Liquid Crystals: Concepts and Physical Properties Illustrated by Experiments* (Taylor & Francis, Boca Raton, FL, 2006).

[32] W. H. de Jeu, B. I. Ostrovskii, and A. N. Shalaginov, Rev. Mod. Phys. **75**, 181 (2003).

[33] R. Lucht, Ch. Bahr, and G. Heppke, J. Phys. Chem. B **102**, 6861 (1998).

[34] R. Stannarius and C. Cramer, Europhys. Lett. **42**, 43 (1998).

[35] N. A. Clark, A. Eremin, M. A. Glaser, N. Hall, K. Harth, C. Klopp, J. E. Maclennan, C. S. Park, R. Stannarius, P. Tin, W. N. Thurmes, and T. Trittel, Adv. Space Res. **60**, 737 (2017).

[36] C. Klopp, T. Trittel, A. Eremin, K. Harth, R. Stannarius, C. S. Park, J. Maclennan, and N. A. Clark, Soft Matter **15**, 8156 (2019).

[37] H. Schüring and R. Stannarius, Langmuir **18**, 9735 (2002).

[38] P. V. Dolganov, P. Cluzeau, and V. K. Dolganov, Liquid Crystals Rev. **7**, 1 (2019).

[39] E. S. Pikina, B. I. Ostrovskii, and S. A. Pikin, Soft Matter **16**, 4591 (2020).

[40] M. I. Godfrey and D. H. Van Winkle, Phys. Rev. E **54**, 3752 (1996)

[41] J. Birnstock and R. Stannarius, Mol. Cryst. Liq. Cryst. Sci. Technol. A **366**, 815 (2001)

[42] T. Trittel, K. Harth, C. Klopp, and R. Stannarius, Phys. Rev. Lett. **122**, 234501 (2019).

[43] R. Stannarius, T. Trittel, Ch. Klopp, A. Eremin, K. Harth, N. Clark, C. S. Park, and J. E. Maclennan, New J. Phys. **21**, 063033 (2019).

[44] W. Helfrich, Phys. Rev. Lett. **23**, 372 (1969)

[45] E. I. Kats and V. V. Lebedev, *Fluctuational Effects in the Dynamics of Liquid Crystals* (Springer, Berlin, 1993).

[46] M. Kléman and O. D. Lavrentovich, *Soft Matter Physics: An Introduction* (Springer-Verlag, New York 2003).

[47] E. S. Pikina, B. I. Ostrovskii, and S. A. Pikin, Eur. Phys. J. E **44**, 81 (2021).

[48] B. M. Ocko, A. Braslau, P. S. Pershan, J. Als-Nielsen, and M. Deutsch, Phys. Rev. Lett. **57**, 94 (1986).

[49] J. Als-Nielsen, Physica A **140**, 376 (1986).

[50] R. Lucht and Ch. Bahr, Phys. Rev. Lett. **78**, 3487 (1997).

[51] F. Picano, P. Oswald, and E. Kats, Phys. Rev. E **63**, 021705 (2001).

[52] E. S. Pikina, B. I. Ostrovskii, and W. H. de Jeu, Eur. Phys. J. E **38**, 13 (2015).

[53] The parameters of the spherical segments of the drop are determined from the condition of minimum of its surface energy $F_s = 2\pi\gamma[R_{\rm cap}^2 + (H/2)^2] + 2\gamma_{\rm A}(S_f - \pi R_{\rm cap}^2)$, provided that the volume of the droplet $V_{dr} = \pi(H/2)[R_{\rm cap}^2 + (H/2)^2/3] + \pi 2hR_{\rm cap}^2$ is fixed. Here S_f is the total area of the FSSF, $R_{\rm cap}$ and (H) are the base radius and the height of the drop, respectively, h is a half of the film thickness, and γ, $\gamma_{\rm A}$ are interfacial tensions defined in the text.

[54] N. N. Lebedev, *Special Functions and Their Applications* (Prentice-Hall, Englewood Cliffs, NJ, 1965).

[55] N. N. Lebedev, I. P. Skalskaya, and Y. S. Uflyand, *Problems of Mathematical Physics* (Prentice-Hall, Englewood Cliffs, NJ, 1965).

[56] J. Happel and H. Brenner, *Low Reynolds Number Hydrodynamics* (Martinus Nijhoff, Leiden, 1973).

[57] P. G. de Gennes and J. Prost, *Physics of Liquid Crystals* (Clarendon Press, Oxford, 1993).

[58] The above formalism of dislocation formation and growth is applicable not only for smectics formed by liquid crystal molecules, but for other lamellar systems, for example, formed in block copolymers, see M. S. Turner, M. Maaloum, D. Ausserré, J.-F. Joanny, and M. Kunz, J. Phys. II France **4**, 689 (1994).

[59] W. H. de Jeu, A. Fera, and B. I. Ostrovskii, Eur. Phys. J. E **15**, 61 (2004).

[60] J. C. Géminard, R. Hołyst, and P. Oswald, Phys. Rev. Lett. **78**, 1924 (1997).

[61] P. Oswald, F. Picano, and F. Caillier, Phys. Rev. E **68**, 061701 (2003).

[62] J. S. Langer and M. E. Fisher, Phys. Rev. Lett. **19**, 560 (1967).

[63] P. S. Pershan and J. Prost, J. Appl. Phys. **46**, 2343 (1975).

[64] Using a general approach proposed by Langer and Fisher [62] (see also [63]), the frequency of thermal generation of any type of critical nucleus of energetically favorable defect or structural unit can be expressed as [39,52]

$$\widetilde{\nu} \cong \exp[(W_c^* - W^{(cr)})/(k_B T)], \tag{G4}$$

where $\widetilde{\nu} = \nu\,({\rm s\,cm^2})$ is the number of thermal nucleations during 1 s per 1 cm^2, $W_c^* \approx \ln[\widetilde{\nu}_0]k_BT$ is a "threshold" activation energy ($W_c^* \approx 60k_BT \sim 2.5\times10^{-19}$ J), and $\widetilde{\nu}_0 = \nu_0$ (s cm^2). The condition for nucleation of one nucleus of more energetically favorable phase or structure of the critical radius R_c, in 1 s over 1 cm^{-2} is then $W^{(cr)} = W_c^*$. For $W^{(cr)} \lesssim W_c^*$ the probability for nucleating of critical nucleus is high, while for $W^{(cr)} > W_c^*$ it is negligible.

[65] E. S. Pikina and B. I. Ostrovskii, Eur. Phys. J. E **40**, 24 (2017).

[66] The estimation of Marangoni force for Ma = 1, $d_0\sigma_{Ma} \sim d_0\partial\gamma/\partial x \sim 10^{-10}\,{\rm J\,m^{-2}} \ll E_d/R_c \sim 10^{-6}$–$10^{-5}{\rm Jm^{-2}}$, demonstrates that Marangoni force can affect only the growing and

moving of dislocation loops with the radius exceeding the critical one to the bounding meniscus of the drop (where E_d is the excess line energy of the elementary dislocation, $E_d \sim 10^{-13}\mathrm{Jm}^{-1}$ [52,65]). Note also that the value $\mathrm{Ma} = 1$ corresponds to the drops of the height $H \sim 10\mu\mathrm{m}$ under action of the temperature gradient $A = 10^{-2}\mathrm{K}/\mu\mathrm{m}$ or $A = 10^{-5}\mathrm{K/nm}$. Thus, the difference between the neighboring regions is very small: 10^{-4}–10^{-3} K, which is not enough for a long process of thickening.

[67] F. Caillier and P. Oswald, Eur. Phys. J. E **20**, 159 (2006).

[68] L. D. Landau and E. M. Lifshitz, *Theory of elasticity* (Butterworth-Heinemann, Oxford 1986).

[69] J. R. A. Pearson, J. Fluid Mech. **4**, 489 (1958).

[70] L. D. Landau and E. M. Lifshitz, *Fluid Mechanics* (Butterworth-Heinemann, Oxford 1987).

[71] M. A. Anisimov, *Critical Phenomena in Liquids and Liquid Crystals* (CRC Press, Boca Raton, FL, 1991).

[72] $H \sim 10\mu\mathrm{m}$, $\beta = 3 \times 10^{-4}\mathrm{K}^{-1}$, $\alpha \sim 0.5 \times 10^{-9}\,\mathrm{Pa}^{-1}$, viscosity $\eta \simeq 1.4 \times 10^{-2}\,\mathrm{kg\,m^{-1}\,s^{-1}}$ [39]), temperature coefficient of surface tension $\varsigma \sim 5 \times 10^{-5}\mathrm{Jm}^{-2}\mathrm{K}^{-1}$ [43], $\gamma \sim \gamma_{\mathrm{A}} \sim 10^{-2}\mathrm{Jm}^{-2}$ [65] and references therein; temperature conductivity $\chi = \varkappa/(\rho_0 C_p) = 4 \times 10^{-8}\,\mathrm{m^2 s^{-1}}$, where $\rho_0 \sim 1.0 \times 10^3\mathrm{kg\,m}^{-3}$[39], $\varkappa \sim 0.12$ J (s m K)$^{-1}$ [71], and $C_p \sim 2.5 \times 10^3$ J (kg K)$^{-1}$ [71] are fluid density, thermal conductivity, and specific heat, respectively.

[73] G. Falkovich, *Fluid Mechanics*, 2nd ed. (Cambridge University Press, Cambridge, 2018).

[74] F. Tisseur and K. Meerbergen, SIAM Rev. **43**, 235 (2001).

[75] Z. Liu, *Multiphysics in Porous Materials* (Springer International Publishing, Cham, 2018).

[76] M. Yamamoto, J. Aerosol Res. **21**, 51 (2006).